USGS
science for a changing world

Groundwater Dynamics at Kīlauea Volcano and Vicinity, Hawai‘i

Chapter F of
The 2008–2018 Summit Lava Lake at Kīlauea Volcano, Hawai‘i

Professional Paper 1867

U.S. Department of the Interior
U.S. Geological Survey

Cover. U.S. Geological Survey aerial photograph toward the northeast of Kīlauea Caldera showing a drill rig at the National Science Foundation (NSF) research drill hole on the summit of Kīlauea (commonly referred to as the Keller well) during the cleanout operation in 1998. The drill hole is approximately 1 kilometer south of the pre-2018 Halemaʻumaʻu Crater and was drilled to a depth of 1,262 meters relative to the derrick floor at 1,102 meters elevation in 1973. The lava flow between the drill rig and Halemaʻumaʻu Crater was emplaced in September 1982 and the lava flow in the foreground was emplaced in September 1971.

Groundwater Dynamics at Kīlauea Volcano and Vicinity, Hawai‘i

By Shaul Hurwitz, Sara E. Peek, Martha A. Scholl, Deborah Bergfeld, William C. Evans, James P. Kauahikaua, Stephen B. Gingerich, Paul A. Hsieh, R. Lopaka Lee, Edward F. Younger, and Steven E. Ingebritsen

Chapter F of
The 2008–2018 Summit Lava Lake at Kīlauea Volcano, Hawai‘i
Edited by Matthew Patrick, Tim Orr, Don Swanson, and Bruce Houghton

Professional Paper 1867

U.S. Department of the Interior
U.S. Geological Survey

U.S. Department of the Interior
DAVID BERNHARDT, Secretary

U.S. Geological Survey
James F. Reilly II, Director

U.S. Geological Survey, Reston, Virginia: 2021

For more information on the USGS—the Federal source for science about the Earth, its natural and living resources, natural hazards, and the environment—visit https://www.usgs.gov or call 1–888–ASK–USGS.

For an overview of USGS information products, including maps, imagery, and publications, visit https://store.usgs.gov.

Suggested citation:
Hurwitz, S., Peek, S.E., Scholl, M.A., Bergfeld, D., Evans, W.C., Kauahikaua, J.P., Gingerich, S.B., Hsieh, P.A., Lee, R.L., Younger, E.F., and Ingebritsen, S.E., 2021, Groundwater dynamics at Kīlauea Volcano and vicinity, Hawai'i, chap. F *of* Patrick, M., Orr, T., Swanson, D., and Houghton, B., eds., The 2008–2018 summit lava lake at Kīlauea Volcano, Hawai'i: U.S. Geological Survey Professional Paper 1867, 28 p., https://doi.org/10.3133/pp1867F.

Associated data for this publication:
Hurwitz, S., Peek, S., Younger, E.F., and Lee, R.L., 2019, Water level, temperature, and chemistry in a deep well on the summit of Kīlauea Volcano, Hawai'i: U.S. Geological Survey data release, https://doi.org/10.5066/P9UCGT2F.

ISSN 1044-9612 (print)
ISSN 2330-7102 (online)

Contents

Figures

Abbreviations

a.s.l.	above sea level
b.s.l.	below sea level
°C	degree Celsius
cm	centimeter
δD	hydrogen stable-isotope composition
$\delta^{18}O$	oxygen stable-isotope composition
HSDP	Hawaii Scientific Drilling Project
k_x	horizontal permeability
k_z	vertical permeability
km	kilometer
km^2	square kilometer
km^3/yr	cubic kilometer per year
L/s	liter per second
Ma	mega-annum
m	meter
m^2	square meter
m^3	cubic meter
m^3/s	cubic meter per second
mg/L	milligram per liter
mW/m^2	milliwatt per square meter
MW	megawatt
m/yr	meter per year
NSF	National Science Foundation
‰	per mil
SOH	scientific observation hole
SP	self potential
TDS	total dissolved solid
TIR	thermal infrared
W/m·K	watt per meter per kelvin

Groundwater Dynamics at Kīlauea Volcano and Vicinity, Hawai‘i

By Shaul Hurwitz, Sara E. Peek, Martha A. Scholl, Deborah Bergfeld, William C. Evans, James P. Kauahikaua, Stephen B. Gingerich, Paul A. Hsieh, R. Lopaka Lee, Edward F. Younger, and Steven E. Ingebritsen

Abstract

Kīlauea Volcano, on the Island of Hawai‘i, is surrounded and permeated by active groundwater systems that interact dynamically with the volcanic system. A generalized conceptual model of Hawaiian hydrogeology includes high-level dike-impounded groundwater, very permeable perched and basal aquifers, and a transition (mixing) zone between freshwater and saltwater. Most high-level groundwater is associated with the low-permeability intrusive complexes that underlie volcanic rift zones and calderas and also act to compartmentalize the groundwater system. Hydrogeologic studies of Kīlauea in recent decades, accompanied by deep research drilling, have shown that high-level groundwater is more widespread than once understood, that permeability decreases dramatically at depth, particularly in rift zones, and that freshwater can occur at depths of as much as several kilometers below the local water table. Copious groundwater recharge causes near-surface conductive heat flow to be near zero over much of Kīlauea. Approximately 95 percent of groundwater discharge occurs offshore, accompanied by approximately 99 percent of the approximately 6,000 megawatts of heat supplied by magmatic intrusion. Here, we summarize current understanding of the groundwater system of Kīlauea Volcano and describe transient changes during the decade or more preceding the 2018 eruption sequence. The changes in groundwater chemistry and thermal structure beneath Kīlauea summit hold implications for volcanic-volatile transport and the potential for explosive volcanism. Between 2008 and 2018, the magma conduit beneath the lava lake likely created an adjacent zone of very hot rock that significantly delayed liquid groundwater inflow to the draining magma conduit. Sulfate concentrations in groundwater beneath Kīlauea summit, sampled at the National Science Foundation-funded drill hole 1.5 kilometers south-southwest of the lava lake, declined substantially between 2010 and present. This decline likely reflects, at least in part, the decreased effectiveness of volatile condensation and solution into groundwater (scrubbing). The vent opening in 2008 presumably focused volatile flux into the vicinity of the vent, and progressive drying of the surroundings further restricted interaction with the groundwater system. The decrease in sulfate concentrations in the drill hole between 2010 and 2018 likely reflects decreased effectiveness of scrubbing.

Introduction

The hydrogeology of Kīlauea Volcano, on the Island of Hawai‘i, has been systematically studied for more than a century. Early work was motivated mainly by local water-supply issues (for example, Martin and Pierce, 1913; Stearns and Clark, 1930; Stearns and Macdonald, 1946), but also constituted some of the first comprehensive hydrogeologic studies of volcanic terrane, highlighting the unique nature of hydrologic conditions in the Hawaiian Islands. O.E. Meinzer, in a report by Stearns and Clark (1930), writes

> To a person who is familiar only with the mainland, the hydrologic conditions in the Hawaiian lslands seem to be freakish in every respect … The rainfall differs from anything found on the mainland in both intensity and areal variability … The islands consist of great volcanoes … Generally speaking, the lava rock is like a sieve … The hydrologic consequences of the widespread occurrence of this very permeable rock are obvious—rapid absorption and downward percolation of the rain water; small and flashy runoff; . . . great ground-water recharge and large supply of ground water; very low and flat water table with great depths to ground water in most places; copious springs in the low valleys, along the coasts, and on the adjacent sea bottom; and salt water at no great depth below the water table.

Though the importance of water-supply issues persists, since about 1970, many hydrogeologic studies of Kīlauea have also been motivated by geothermal resources and groundwater-volcano interactions. Although O.E. Meinzer’s early observations remain relevant and broadly correct, data from deep drill holes and modern geophysical and water-chemistry methods challenge elements of the classic conceptual model: high-level groundwater, though not ubiquitous, is more widespread than once believed; permeability decreases dramatically at depth

within intrusive complexes; and freshwater has been found at depths of as much as several kilometers below the local water table. These new observations inform current understanding of groundwater-volcano interactions.

Hydrogeologic Framework of the Groundwater System

The Island of Hawai‘i is built mainly of basaltic lava flows erupted from large shield volcanoes, and great piles of thin lava flows form highly permeable aquifers (Stearns and Clark, 1930). Dense intrusive complexes built by near-vertical diking in volcanic rift zones are substantially less permeable than the porous surficial flows. Some of the ash and soil horizons interlayered with the lava flows are also less permeable, because of compaction and lithification, and thick lava flows that ponded in preexisting depressions also tend to be less permeable than stacks of thin flows (Izuka and others, 2018).

The rift zones of Mauna Loa (fig. 1) bound the regional groundwater system that encompasses Kīlauea Volcano, and the area bounded by the rift zones of Kīlauea forms a partly isolated subsystem. Precipitation and groundwater recharge vary greatly across Kīlauea, most streamflow is ephemeral, and the vast majority of groundwater discharges below sea level (Stearns and Macdonald, 1946).

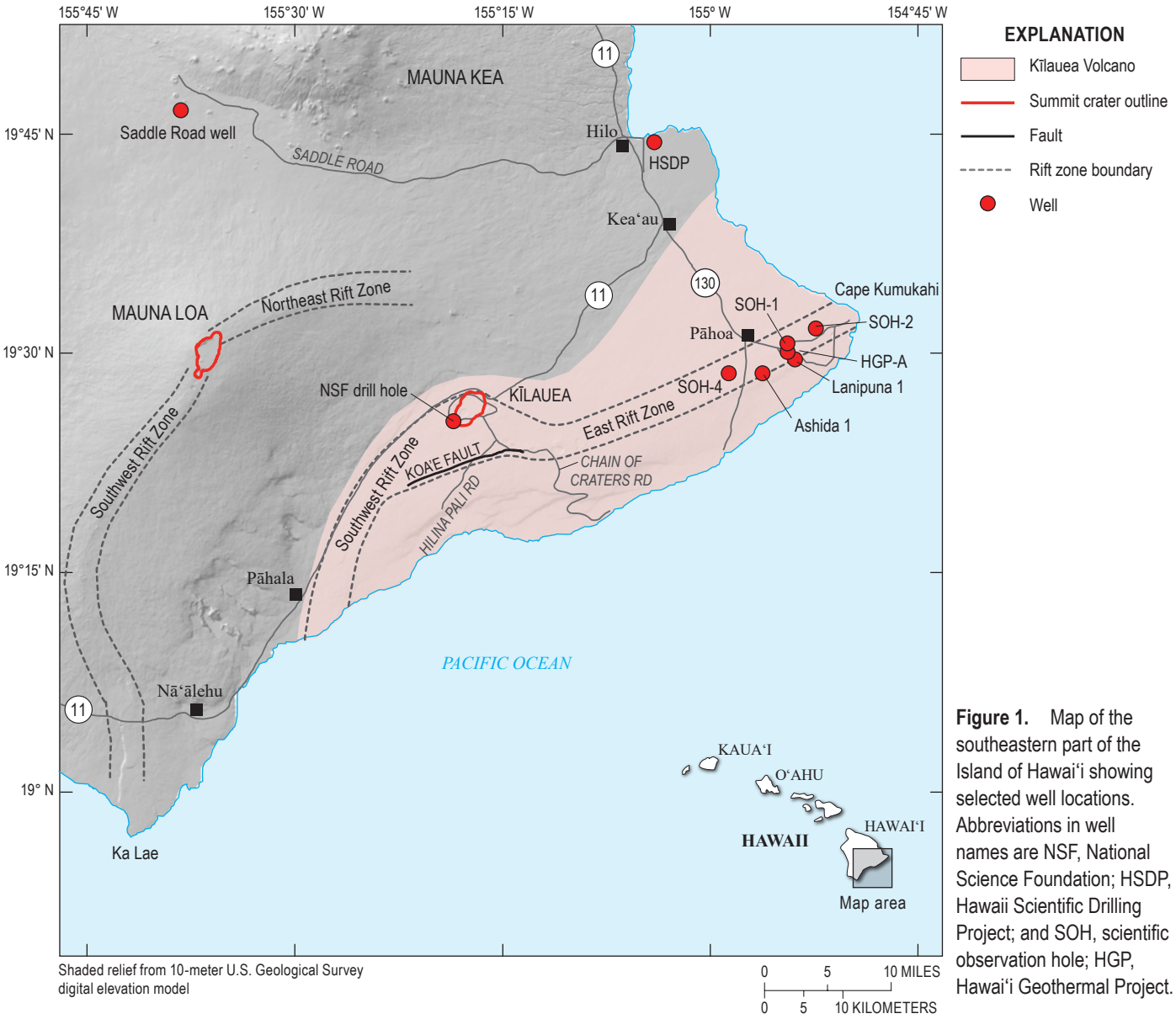

Figure 1. Map of the southeastern part of the Island of Hawai‘i showing selected well locations. Abbreviations in well names are NSF, National Science Foundation; HSDP, Hawaii Scientific Drilling Project; and SOH, scientific observation hole; HGP, Hawai‘i Geothermal Project.

Groundwater Occurrence and Water-Table Configuration

A generalized conceptual model of Hawaiian hydrogeology includes high-level dike-impounded groundwater, perched aquifers, a basal freshwater lens, and a transition (mixing) zone between freshwater and saltwater (fig. 2*A*). Most high-level groundwater is associated with the intrusive complexes that underlie volcanic rift zones and calderas (fig. 2*B*).

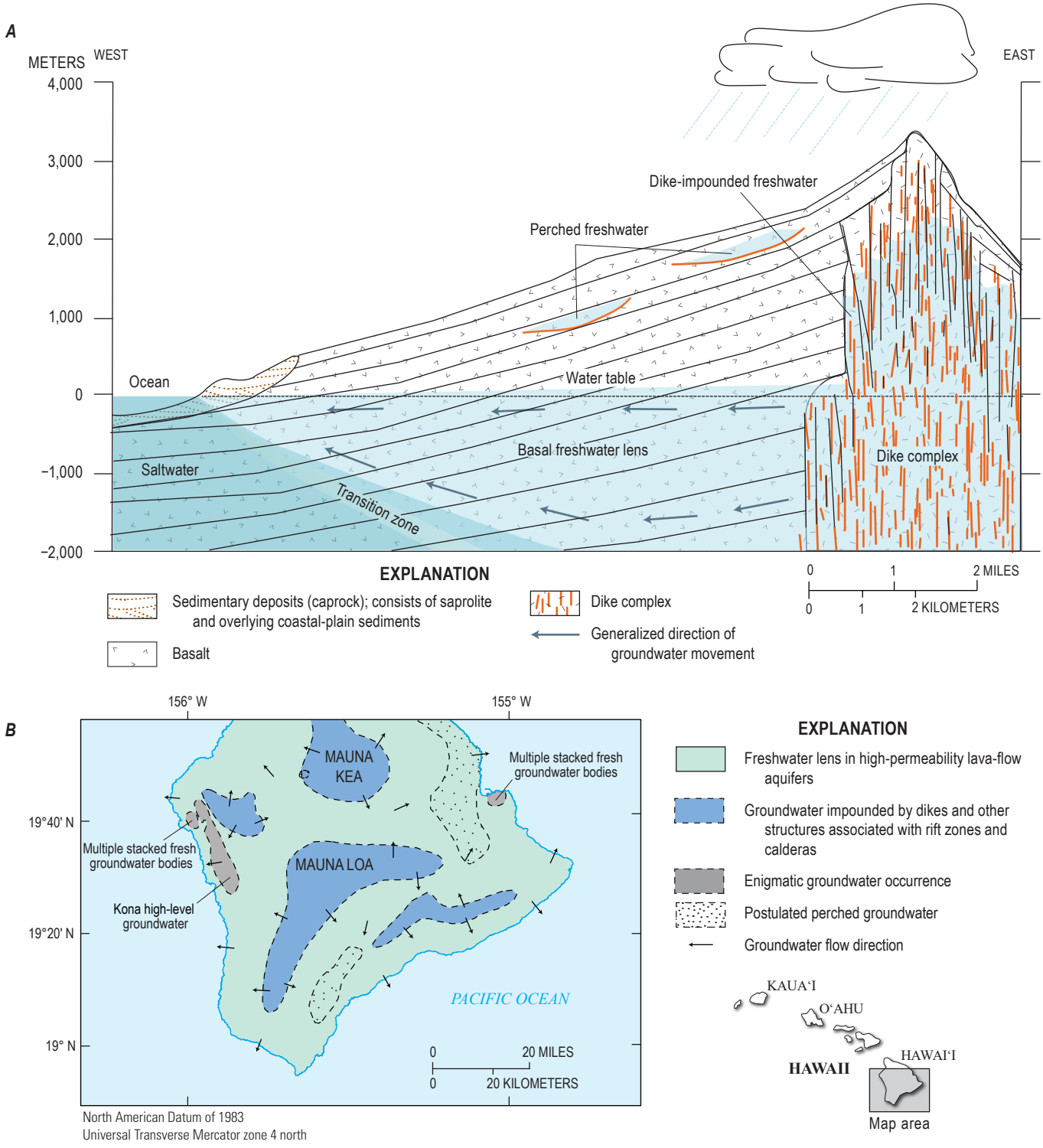

Figure 2. *A*, Generalized conceptual model of volcanic-island hydrogeology showing dike-impounded water, perched aquifers, a basal freshwater lens, and a transition (mixing) zone between freshwater and saltwater (Pierce and Thomas, 2009). *B*, Map of groundwater modes on the Island of Hawai'i. Figure after Izuka and others (2018).

In the late l9th century, W. Badon Ghyben and A. Baurat Herzberg showed that, under hydrostatic conditions and at standard temperature (25 °C), the configuration of the basal freshwater lens within permeable oceanic islands is a function of the relative density of freshwater and saltwater and of the altitude of the water table above sea level—if the water table stands 1 meter (m) above sea level (a.s.l.), then saltwater should be encountered approximately 40 m below sea level (b.s.l.). Though the Ghyben-Herzberg assumptions are violated in essentially all real systems, they provide useful approximations for many small islands and for parts of Hawai‘i. The slope of the basal water table within highly permeable Hawaiian basalts is generally very shallow; Peterson (1981) cited an average value of 0.001 for the Hawaiian Islands.

The existence of dike-impounded water substantially above the basal freshwater lens was first documented in the Hawaiian Islands during construction of the Waiāhole tunnel on O‘ahu in 1913–1915, where head differences of about 50 m were measured across 1- to 4-m-thick dikes (O.E. Meinzer in Stearns and Clark, 1930). The first direct evidence for impounded water on the Island of Hawai‘i itself was obtained in 1946, when an inclined shaft encountered the water table at 70 m a.s.l. near Pāhala (fig. 1), a location where the basal water table would be only approximately 1.5–3 m a.s.l. under Ghyben-Herzberg assumptions. The water level measured in the Pāhala shaft corresponds with a coherent, laterally extensive, low-electrical-resistivity layer (Hussong and Cox, 1967).

Recent estimates of the extent of dike-impounded groundwater on the Island of Hawai‘i are shown in figure 2*B*, and direct and indirect evidence for high-level water-table elevations is summarized in figure 3. The highest water-table elevation measured to date is 1,390 m a.s.l. in the saddle between Mauna Loa and Mauna Kea, where even higher artesian heads occur in wells (Thomas and others, 2015). The water-table elevation beneath the summit of Kīlauea, first measured in 1973 (Zablocki and others, 1974; Keller and others, 1979) and monitored intermittently by the U.S. Geological Survey over the succeeding decades (Hurwitz and others, 2019), is approximately 600 m a.s.l. Both in the saddle region (Pierce and Thomas, 2009) and at Kīlauea summit (Kauahikaua, 1993; Revil and others, 2018), as at Pāhala, the measured water-table elevation approximately corresponds to coherent, laterally extensive, low-resistivity layers. Near the coastline at Hilo—where the Ghyben-Herzberg relation suggests the freshwater-saltwater transition is at depths of tens of meters below sea level—the Hawaii Scientific Drilling Project (HSDP) borehole encountered freshwater entries at depths as great as 3 kilometers (km) b.s.l. (Stolper and others, 2009). Models that successfully reproduce both

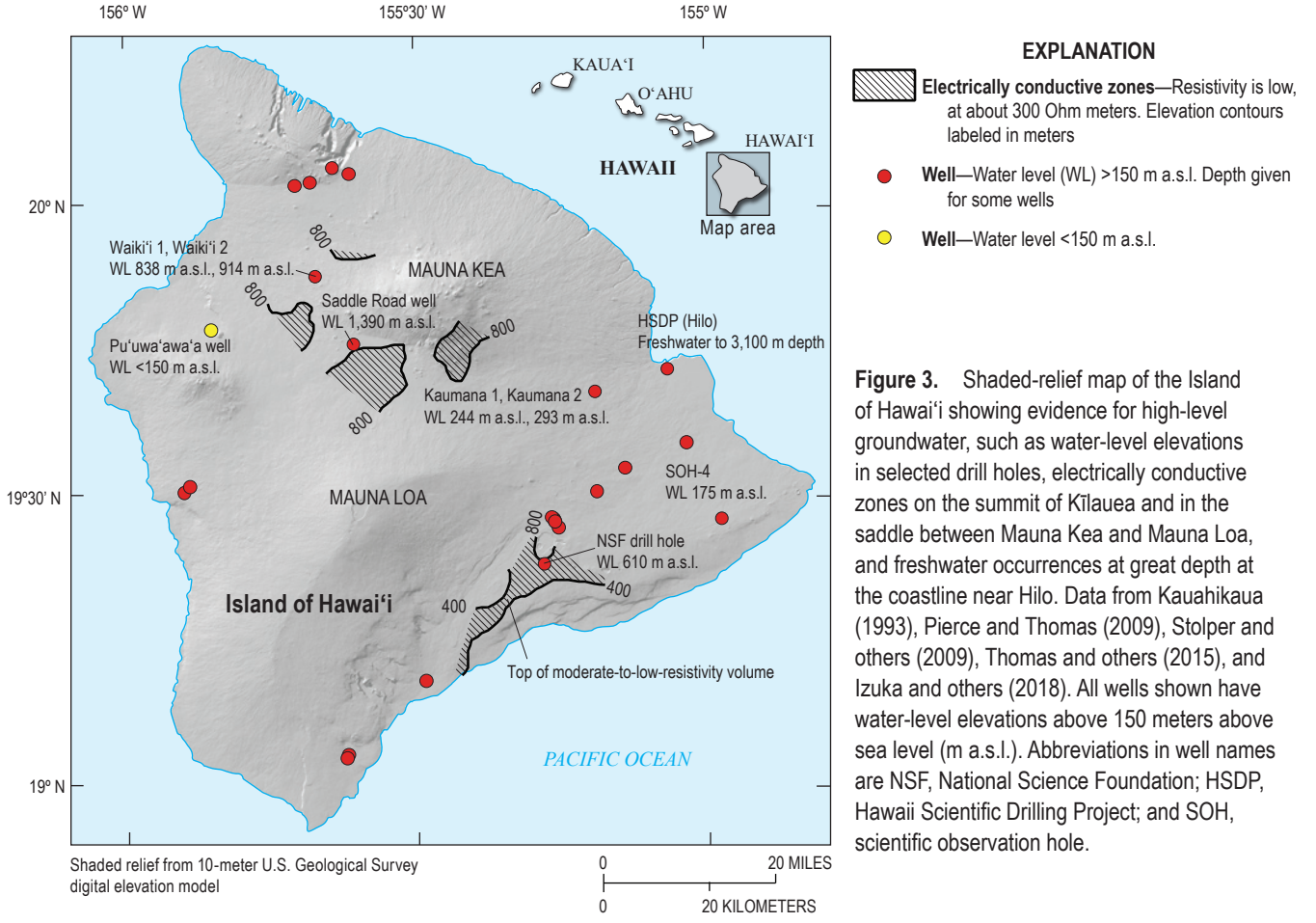

Figure 3. Shaded-relief map of the Island of Hawai‘i showing evidence for high-level groundwater, such as water-level elevations in selected drill holes, electrically conductive zones on the summit of Kīlauea and in the saddle between Mauna Kea and Mauna Loa, and freshwater occurrences at great depth at the coastline near Hilo. Data from Kauahikaua (1993), Pierce and Thomas (2009), Stolper and others (2009), Thomas and others (2015), and Izuka and others (2018). All wells shown have water-level elevations above 150 meters above sea level (m a.s.l.). Abbreviations in well names are NSF, National Science Foundation; HSDP, Hawaii Scientific Drilling Project; and SOH, scientific observation hole.

the deep occurrence of freshwater at Hilo and the reduced thermal gradients to depths in excess of 3 km b.s.l. require good hydraulic connection with high-level groundwater in the interior of the island (Buttner and Huenges, 2003).

Thermal Structure, Heat Flow, and Permeability

Heat flow-age models suggest heat-flow values of approximately 50 milliwatts per square meter (mW/m^2) for the 95–90 million year old (Ma) oceanic lithosphere at Hawai‘i (Sclater and others, 1980) and heat-flow measurements around the Hawaiian Islands confirm these values (von Herzen and others, 1989; Harris and others, 2000). The three deep drill holes on the Island of Hawai‘i that do not intercept intrusive complexes (fig. 4, blue profiles) yield similar heat-flow estimates. Assuming a thermal conductivity of 1.8 watts per meter per degree kelvin (W/m·K) (Horai, 1991), deep temperature gradients in west Hawai‘i at Pu‘uwa‘awa‘a (at depths greater than 1.5 km) and Waiki‘i (at depths greater than 1 km) imply heat flows of 35 and 80 mW/m^2, respectively (Kauahikaua, 1993). Assuming a similar thermal conductivity, the deepest section of the Hilo drill hole (greater than 1.5 km depth) yields a heat flow of 31 mW/m^2, suggesting that heat transport by groundwater influences the thermal regime to the total depth of more than 3 km and implying moderately high permeability (approximately 7×10^{-13} square meters [m^2]) to at least that depth (Buttner and Huenges, 2003).

The temperature regime and heat flow are markedly different in the more numerous deep drill holes that intercept intrusive complexes (fig. 4, red and orange profiles).

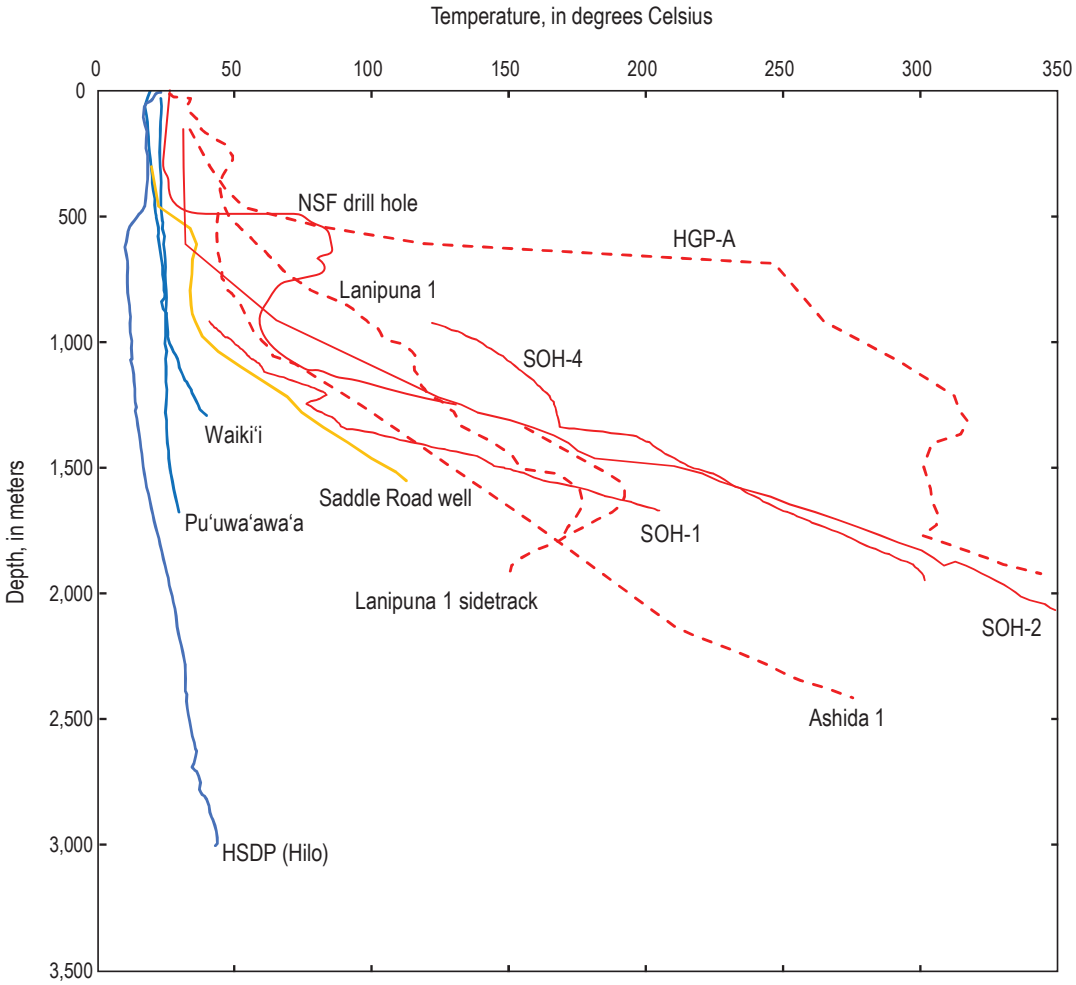

Figure 4. Plot of temperature profiles from deep drill holes on the Island of Hawai‘i. Red lines denote drill holes on the summit and East Rift Zone of Kīlauea, the orange line is the Saddle Road drill hole between Mauna Loa and Mauna Kea, and blue lines denote wells in Hilo and west Hawai‘i. Red dashed lines denote drill holes intended for geothermal-energy production in the lower East Rift Zone. The nearby Scientific Observation Hole (SOH) series was intended to monitor the potential impact of geothermal production. Well locations are shown either on figure 1 or 3. Data from Kauahikaua (1993), Stolper and others (2009), and Thomas and others (2014).

Temperature gradients from the deepest parts of the drill holes at the summit of Kīlauea and along its East Rift Zone yield heat flows of 370–820 mW/m^2 (Kauahikaua, 1993), a full order of magnitude larger than the oceanic background heat flow. More surprisingly, the temperature profile at depths greater than 1 km in the Saddle Road drill hole between Mauna Loa and Mauna Kea yields a heat flow of approximately 260 mW/m^2 for an assumed thermal conductivity of 1.8 W/m·K. This fairly recent and unexpected result suggests that older intrusive complexes on the Island of Hawai‘i may also retain significant heat and, further, that they may be broader and more extensive than previously recognized (Thomas and others, 2014), consistent with gravity modeling (Flinders and others, 2013). Aeromagnetic data over the Island of Hawai‘i have been interpreted in terms of a thin magnetized shell, implying that the deeper core is nonmagnetic, either caused by severe hydrothermal alteration, high temperature, or some combination of the two (Hildebrand and others, 1993, p. 4,114). The unexpectedly high temperatures and heat flow in the Saddle Road well (fig. 4) support the idea that high temperature is the dominant influence, however, there is no obvious correlation between the estimated thickness of the magnetic shell and heat flow estimates from the deep wells.

The absence of large-scale convective circulation implied by the nearly linear temperature gradients at depth in the intrusive complexes (fig. 4), despite high temperatures (100–350 °C) and large temperature gradients (150–320 °C per kilometer), implies bulk permeabilities less than 10^{-14} m^2 (Ingebritsen and Scholl, 1993)—about four to five orders of magnitude lower than the mean permeabilities measured by well tests in shallow Hawaiian basalts (Williams and Soroos, 1973; Rotzoll and others, 2007; Rotzoll and El-Kadi, 2008). Given a representative length of 500 m and temperature difference of 100 °C, a permeability of 10^{-14} m^2 yields a Rayleigh number of about 100 at 250 °C, well above the critical value for the onset of convection. It is not clear whether pervasive intrusion or hydrothermal alteration is the primary cause of the low bulk permeability at depth; both are probably important, and related by the role of dikes as heat sources that drive hydrothermal alteration.

The National Science Foundation (NSF) research drill hole on the summit of Kīlauea (commonly referred to as the Keller well), approximately 1 km south of the edge of the pre-2018 Halema‘uma‘u Crater, was drilled to a depth of 1,262 m relative to the derrick floor at 1,102 m elevation between April 6 and July 9, 1973, and encountered the water table at 491 m depth or approximately 612 m elevation (Keller and others, 1979). The presence of hydrothermal alteration in the NSF drill hole (fig. 5*A*) corresponds to depths below the water table, a pronounced decrease in measured core-scale permeability, and a change in the nature of the temperature profile from nearly isothermal to a distinctive curvature that is subject to a variety of interpretations. Geochemical modeling suggests that the secondary minerals observed in the drill core—mainly calcite, iron-titanium oxides, and calcium-magnesium smectites—precipitated from cooling hydrothermal fluids that equilibrated at temperatures less than 150 °C (fig. 5*B*). Rapid reductions in permeability with depth at temperatures greater than or equal to 30–50 °C have also been observed in volcanic rocks of the Columbia River Basalt Group (Burns and others, 2015) and the Cascade Range (Blackwell and Baker, 1988; Swanberg and others, 1988; Blackwell, 1994; Hulen and Lutz, 1999; Saar and Manga, 2004) and, similarly, been attributed to hydrothermal alteration with pore-clogging minerals.

Several models have been suggested to explain the distinctively curved part of the NSF drill hole temperature profile below the water table (fig. 5*A*): free convection (fig. 6*A*), continuous lateral flow (fig. 6*B*), and transient lateral flow (fig. 6*C*). The steady-state, free-convection model depicted in figure 6*A* matches the observed temperature distribution with a two-dimensional model that has half-cell dimensions of 700 by 700 m, uniform and moderately high permeability (6×10^{-14} m^2) from the water table to 1,200 m depth (approximately 100 m b.s.l.), and zero permeability at greater depth. The upper boundary at 500 m depth, representing the water table, is held at a constant temperature of 20 °C, and the lower boundary at 1,900 m depth is maintained at 650 °C. In this conceptualization, the drill hole intercepted an active hydrothermal convection cell underlain by effectively impermeable rocks (Keller and others, 1979).

The continuous-lateral-flow model (fig. 6*B*) invokes a continuous flux of hydrothermal fluid, active to the present day, through a moderately permeable (greater or equal to 3×10^{-15} m^2) layer at 490–730 m depth. In the transient-lateral-flow model (fig. 6*C*), conductive cooling follows a brief (on the order of 10^2 years) period of lateral flow during which initially high permeability (3×10^{-11} m^2) is progressively diminished by hydrothermal alteration. Because of the slow rate of heat conduction, the thermal perturbations caused by a finite advective disturbance can persist for several thousand years after hydrothermal flow has ceased. Both of the lateral-flow models (figs. 6*B* and 6*C*) are sensitive to initial conditions and, with plausible initial conditions, require 750–1,000 simulation years to match the measured temperature profile in the NSF drill hole. This inferred timing can be compared with the chronology of major volcanic and faulting events at Kīlauea (fig. 6*D*).

All three models for the thermal structure below the water table in the NSF drill hole (fig. 6) invoke conduction-dominated heat flow, and thus low permeabilities (less than or equal to 10^{-16} m^2) at depths greater than approximately 1 km. They all attribute the nearly isothermal temperature profile above the water table to groundwater recharge. In fact, the “great ground-water recharge” first highlighted by O.E. Meinzer (in

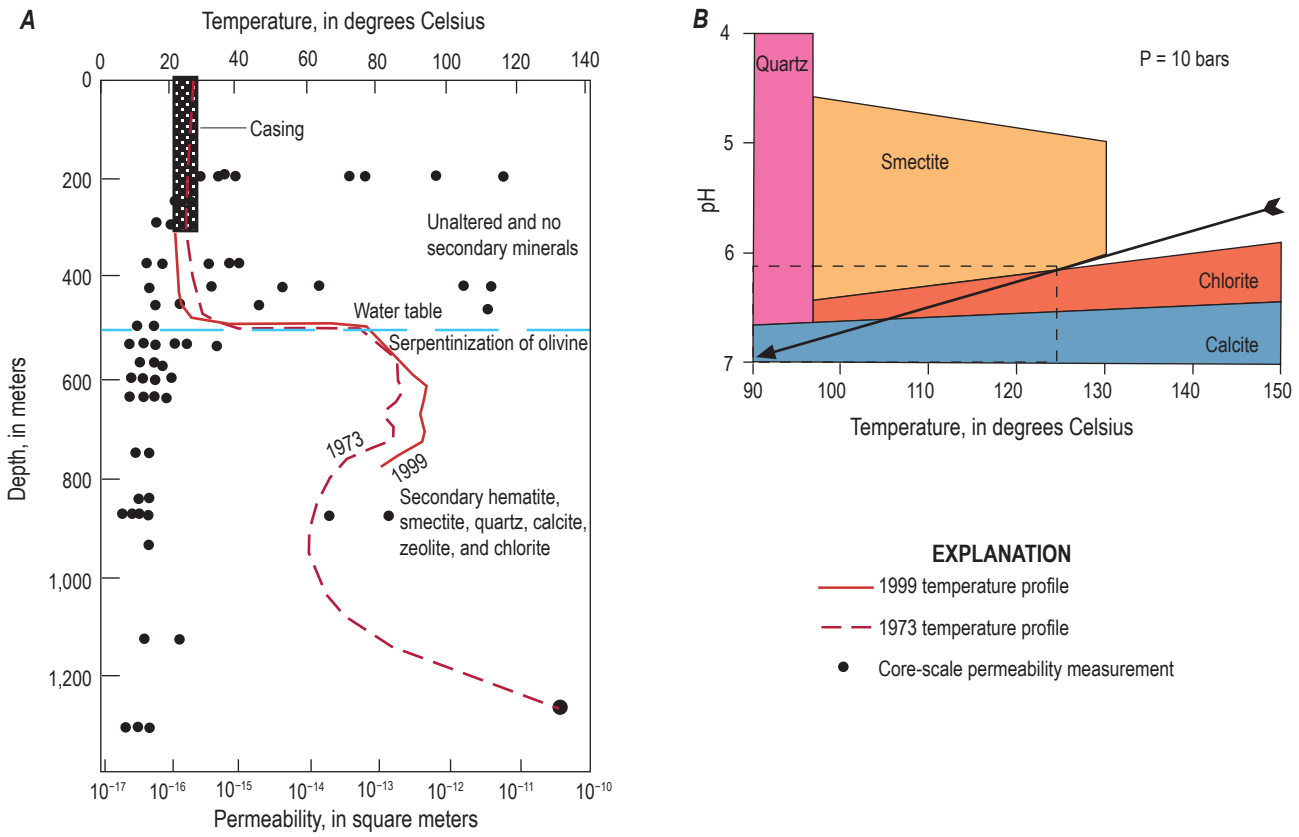

Figure 5. Profile of the National Science Foundation (NSF) drill hole and mineral saturation fields. *A*, Temperature profiles, core-scale permeability measurements, and water-table position in the NSF drill hole on the summit of Kīlauea (after Keller and others, 1979). Descriptions of hydrothermal alteration are also noted. *B,* Calculated mineral supersaturation fields below the water table (at a pressure of 10 bars) over the pertinent ranges of temperature and pH found in the NSF drill hole (Hurwitz and others, 2003). The dashed rectangle represents conditions under which the secondary mineral assemblage below the water table may have formed. The arrow represents the hypothetical evolution of a fluid with progressively lower temperature and increasing pH.

Stearns and Clark, 1930) causes nearly isothermal conditions at shallow depths in most Hawaiian drill holes (fig. 4). Subvertical groundwater downflow at rates of only a few centimeters per year is sufficient to completely suppress conductive heat flow (Bredehoeft and Papadopulos, 1965), and groundwater recharge rates over most of the southeastern part of the Island of Hawai‘i are much higher, on the order of 1 meter per year (m/yr) (fig. 7*A*). Low permeabilities at depth in the intrusive complexes inhibit downward groundwater flow, such that most temperature profiles in the intrusive complexes become quasi-conductive at depths greater than approximately 1 km (fig. 4). External to the intrusive complexes, however, the sparse available data suggest that active groundwater flow can suppress temperatures to much greater depth. Temperatures in the Pu’uwa’awa’a and Hilo drill holes (fig. 4), for instance, appear affected by groundwater circulation to total depths of approximately 1.7 km and greater than 3 km, respectively. The apparent persistence of high permeabilities to greater depth suggests that the geologic sections penetrated by these drill holes cooled rapidly through the temperature range associated with hydrothermal alteration and thereafter were not exposed to temperatures in excess of about 30–50 °C.

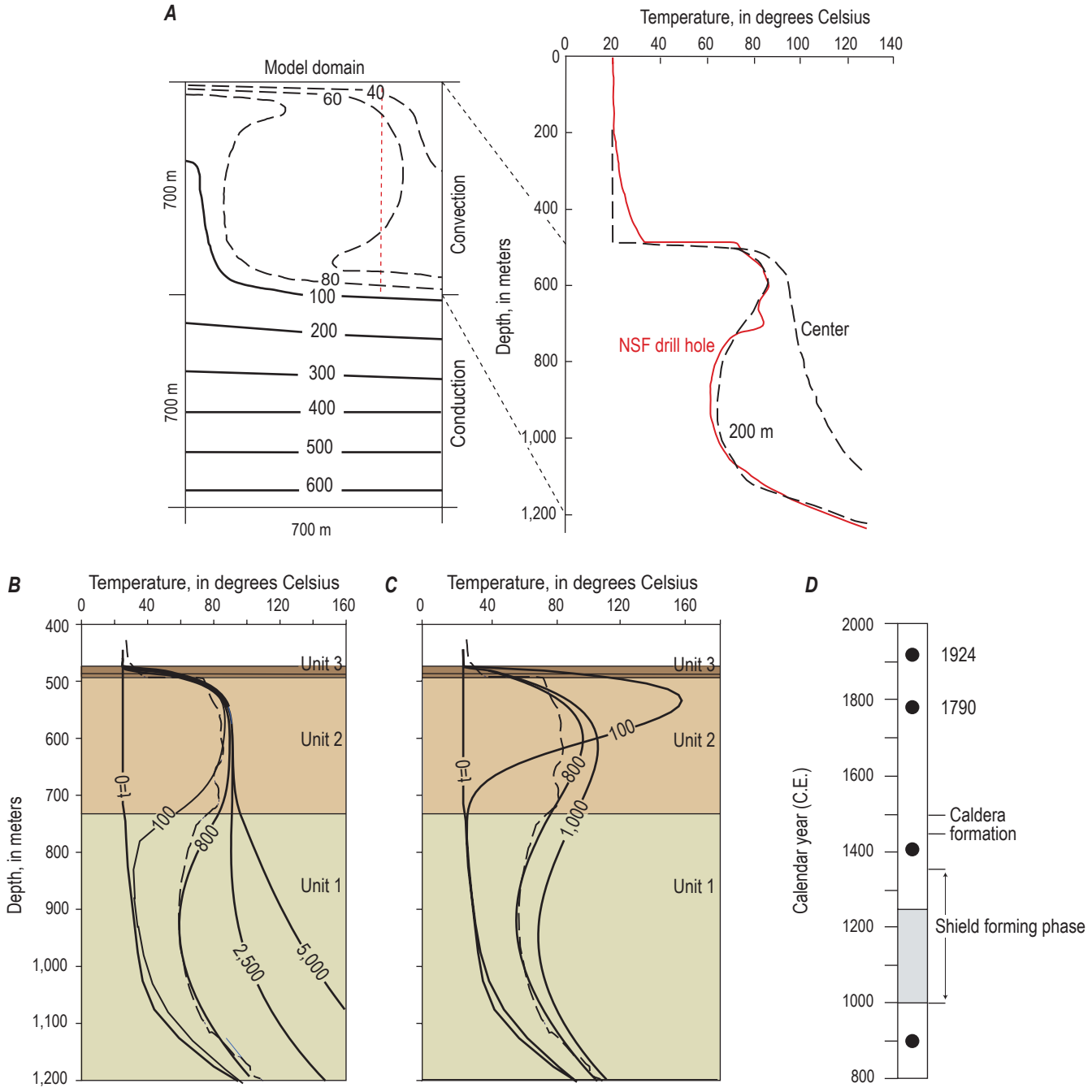

Figure 6. Three models to explain the temperature profile in the National Science Foundation (NSF) drill hole on the summit of Kīlauea. *A*, Model domain and temperature profile for the steady-state free convection model (Murray, 1974; Keller and others, 1979). The left plot shows temperature contours (in degrees Celsius) from a cross-section of the model; distances are in meters (m). The vertical dashed red line represents the position of the NSF drill hole relative to the center of a simulated convection cell. The right plot shows simulated temperature profiles at the center of the convection cell and along the dashed red line. The solid red line shows the measured profile from the NSF drill hole. *B*, Temperature profiles for the continuous lateral flow model (Hurwitz and others, 2002). Simulated temperatures are shown for time (*t*) equals 0, 100, 800, 2,500, and 5,000 years. *C*, Temperature profiles for the transient lateral flow model (Hurwitz and others, 2002). Simulated temperatures are shown for time (*t*) equals 0, 100, 800, and 1,000 years. The dashed line in plots *B* and *C* is the observed NSF drill hole temperature profile from 1973. Plots *B* and *C* indicate that both continuous and transient lateral flow models imply onset of hydrothermal flow in a moderately permeable layer at 490–730 meters depth (unit 2) 750 to 1,000 years prior (1000 to 1250 current era [C.E.]) to match the observed temperature profile. *D*, Chronology of major geologic events at Kīlauea, including a shield-forming phase, explosive eruptions (circles), and onset of the modern caldera subsidence (Mastin and others, 1998; Clague and others, 1999; Hurwitz and others, 2002). The period in gray shows the time interval for the onset of hydrothermal flow as indicated in plots *B* and *C*.

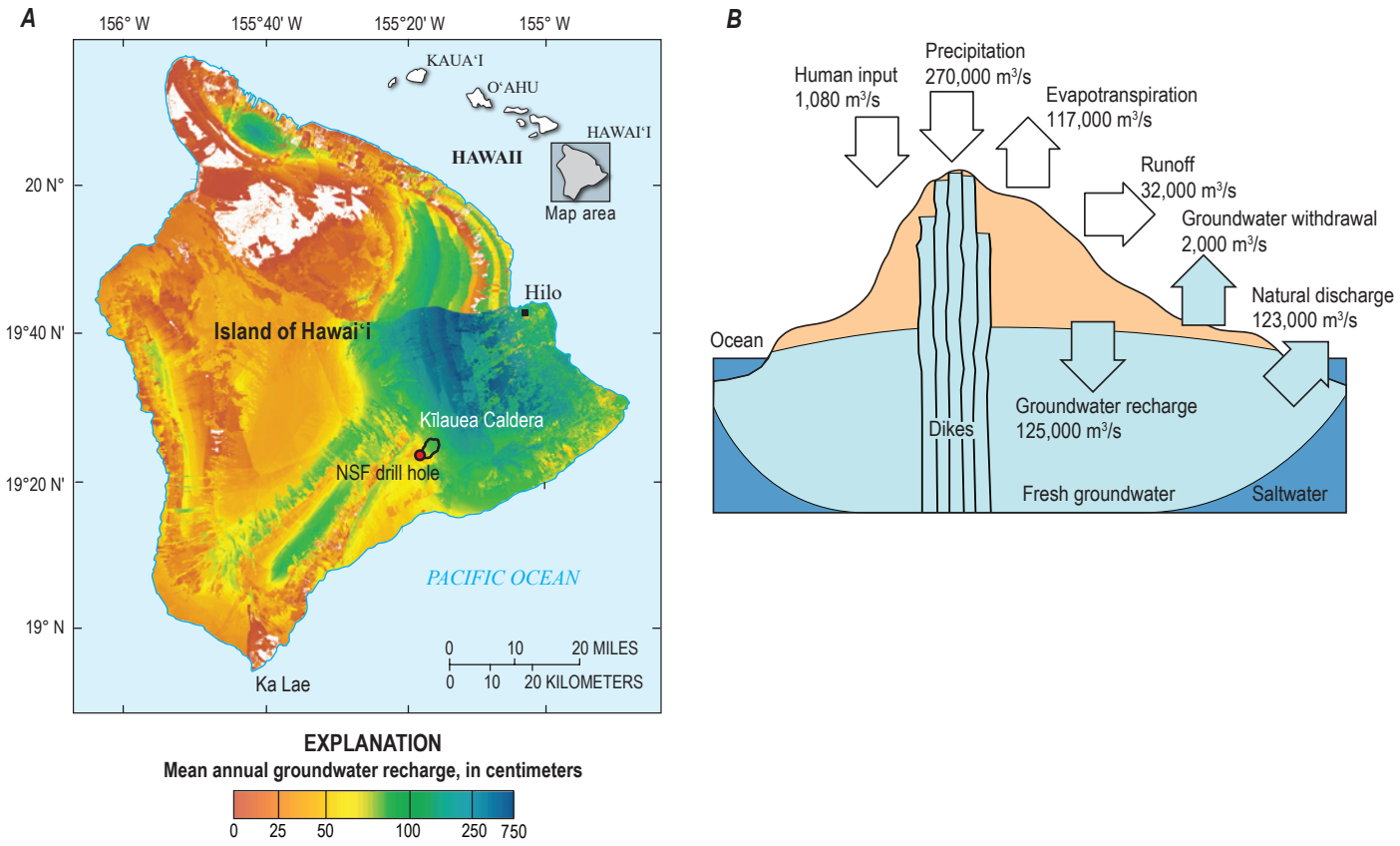

Figure 7. Groundwater recharge and water budget for the Island of Hawai'i. *A*, Map of estimated mean annual groundwater recharge for recent conditions on the Island of Hawai'i (Engott, 2011). *B*, Cartoon showing the estimated water budget for the Island of Hawai'i (Izuka and others, 2018). Values are in cubic meters per second (m^3/s). Precipitation includes rain and fog. Input from human activities includes irrigation and leaks from water-supply, septic, and sewer systems. Runoff includes that from natural surfaces as well as from paved surfaces flowing into storm drains. Natural discharge includes spring flow, stream base flow, and submarine groundwater discharge.

Recharge and Discharge of Groundwater and Heat

Estimated groundwater recharge rates on Kīlauea Volcano generally exceed 0.5 m/yr and locally exceed 2 m/yr (fig. 7*A*), and water-budget studies of the entire Island of Hawai'i estimate that nearly half of the total precipitation recharges the groundwater system (for example, see fig. 7*B*). Comprehensive early inventories found that the total yield of visible springs, tunnels, and wells on Hawai'i amounts to only about 2.5 percent of the total precipitation, and inferred that huge unmeasured amounts of groundwater discharge to the ocean well below sea level (Stearns and Macdonald, 1946).

The shoreline thermal-infrared (TIR) signatures summarized in figure 8*A* document relatively warm groundwater-discharge temperatures along the parts of the shoreline bracketed by Kīlauea's rift zones, reflecting volcanic heat input. Spring temperatures are generally lower than the ambient ocean temperature outside the area bracketed by the rift zones. Because TIR sensing detects thermal radiation only from the uppermost 0.1 millimeter of the water column (Torgerson and others, 2001), and vigorous ocean currents and wave action readily disperse the temperature effects of groundwater discharge, the TIR anomalies in figure 8*A* reflect only groundwater discharge occurring at or very near the shoreline. The freshwater entries observed to more than 3 km depth in the deep drill hole at Hilo (fig. 8*B*; Buttner and Huenges, 2003) suggest that significant submarine groundwater discharge also occurs farther offshore, where it would lack a clear TIR signature.

Onshore observations and measurements (fig. 9) are consistent with the shoreline TIR survey results (fig. 8*A*), showing thermal springs and wells essentially confined to the rift zones and summit of Kīlauea and the downslope area bracketed by the rift zones. The temperature profiles from shallow wells in and just south of the lower East Rift Zone (fig. 9*B*) reflect warmer, less-dense water floating on top of cooler, higher density water (Gingerich, 1995).

Comparison between the subaerial conductive (figs. 4, 8*B*, and 9*B*) and advective (figs. 8*A* and 9) heat discharge and the magmatic heat input to Kīlauea Volcano further suggests that a large fraction of the magmatically supplied heat is transported offshore by deep groundwater flow. The long-term (on the order of 10^2 years) supply rate of basaltic magma to Kīlauea is approximately 0.1 cubic kilometers

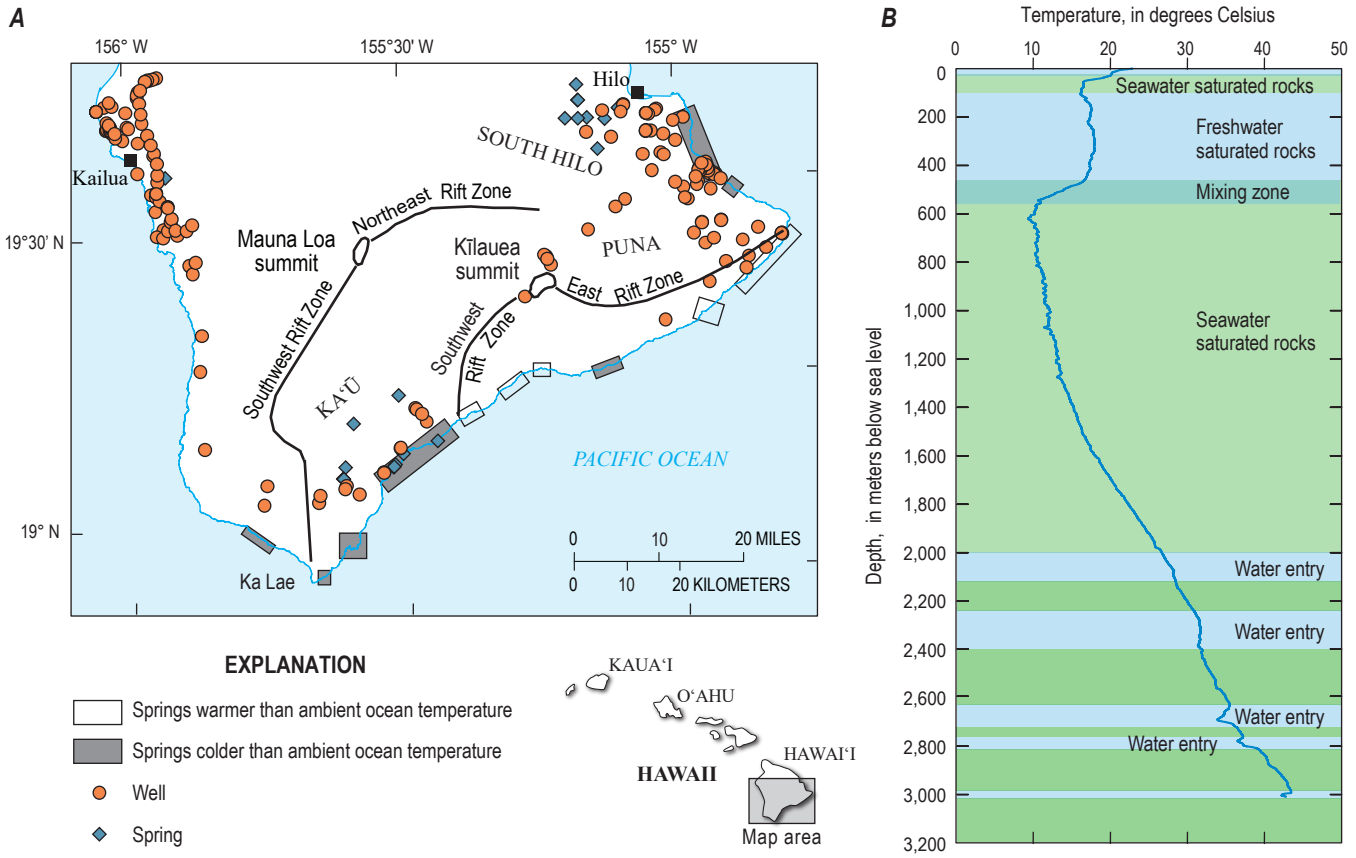

Figure 8. Spring discharge temperatures on the Island of Hawai‘i and temperature profile of the deep Hilo well. *A*, Map of relative spring-discharge temperatures (Fischer and others, 1966) and selected well locations (Takasaki, 1993) in Ka‘ū, Puna, and South Hilo Districts, Island of Hawai‘i. *B*, Temperature profile from the Hawaii Scientific Drilling Project (HSDP) deep research drill hole in Hilo (Stolper and others, 2009). Some of the inflections at depths of 2,200-2,700 meters were associated with water entries (permeable horizons). The Hilo wellhead elevation was a few meters above sea level.

per year (km^3/yr) (Swanson, 1972), of which approximately 0.04 km^3/yr is erupted (about 8 km^3 erupted since 1823) and approximately 0.06 km^3/yr is intruded (D.A. Swanson, U.S. Geological Survey, written commun., July 26, 2019). An intrusion rate of 0.06 km^3/yr translates to a heat supply of more than 6,000 megawatts (MW), assuming a density of 2,800 kilograms per cubic meter (Wright and others, 1976), latent heat of crystallization of 4×10^5 joules per kilogram, and heat capacity of crystallized basalt of 1,000 joules per kilogram per kelvin (Bouhifd and others, 2007), and cooling from 1,100 to 300 °C. Because of the copious groundwater recharge, very little of the heat from intrusion discharges to the land surface via conduction (figs. 4, 8*B*, and 9*B*); onshore conductive heat discharge appears to be negligible. Onshore heat discharge by thermal springs may account for approximately 60 MW, given a half-dozen spring groups discharging a total of approximately 10^3 liters per second (L/s) (Stearns and Macdonald, 1946) at temperatures approximately 15 °C above ambient (Janik and others, 1994; Scholl and others, 1995). Thus, nearly all of the more than 6,000 MW from intrusion likely is discharged by submarine thermal groundwater discharge. It appears that more than 90 percent of solute discharge (Schopka and Derry, 2012), approximately 95 percent of groundwater discharge (Stearns and Macdonald, 1946), and approximately 99 percent of the discharge of intrusion-supplied heat occurs offshore. Total groundwater recharge for the areas that encompass the Southwest Rift Zone and East Rift Zone of Kīlauea is estimated at 4,200 and 22,000 L/s, respectively (Engott, 2011), and this groundwater would need to be heated by an average of approximately 60 °C in order to carry 6,000 MW of heat.

Groundwater Chemistry

Geochemical observations provide further insight regarding volcano-groundwater interactions. The stable-isotope composition of groundwater makes it possible to infer patterns of subsurface flow and processes between recharge areas and discharge points. Solute concentrations that vary in time and space reflect dynamic interaction between the volcanic and groundwater systems.

Results from a comprehensive study of the stable-isotope composition of precipitation and groundwater done in the early 1990s help to constrain patterns of groundwater flow in Kīlauea Volcano and vicinity. A network of as many as

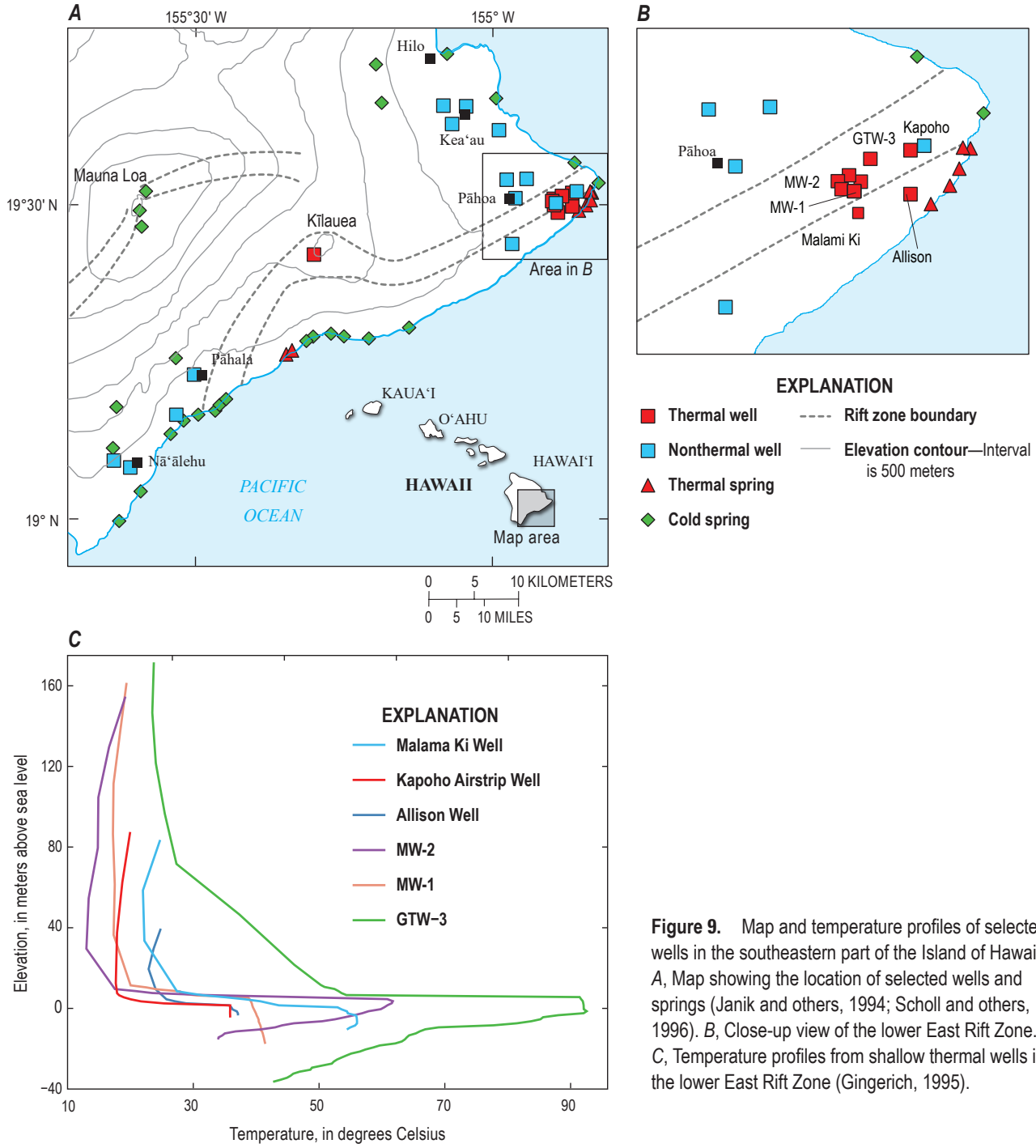

Figure 9. Map and temperature profiles of selected wells in the southeastern part of the Island of Hawai'i. *A*, Map showing the location of selected wells and springs (Janik and others, 1994; Scholl and others, 1996). *B*, Close-up view of the lower East Rift Zone. *C*, Temperature profiles from shallow thermal wells in the lower East Rift Zone (Gingerich, 1995).

66 precipitation collectors was emplaced in a 4,200-square-kilometer (km^2) area bounded by Ka Lae, Mauna Loa summit, and Hilo (figs. 1 and 10) and sampled twice yearly for a 3-year period (August 1991 to August 1994). Stable isotopes in precipitation revealed three distinct isotopic gradients with elevation that are correlated with trade-wind, rain-shadow, and high-elevation climatological patterns (fig. 11). During the same time period, groundwater was sampled yearly in coastal springs, wells, and high-elevation springs. The flow paths in figure 12 were drawn by comparing the isotopic composition of groundwater, corrected, if necessary, for a seawater component, with the volume-weighted-average isotopic composition of precipitation. The hypothetical elevation range of recharge contributions to groundwater discharge at the sampling point is shown as (1) the elevation at which rainfall volume-weighted-average composition matches groundwater composition and (2) the elevation range representing integrated recharge along the flow path. Flow

lines are drawn perpendicular to topography, unless geologic and isotopic evidence suggest otherwise (Scholl and others, 1996). The areal contrasts in stable isotopes are consistent with the concept that the volcanic rift zones compartmentalize the regional groundwater system, isolating the groundwater-flow system south of Kīlauea's summit and rift zones. Part of the Southwest Rift Zone appears to act as a conduit for water from higher elevation, but there is no isotopic evidence for downrift flow in the springs and shallow wells sampled in and near the lower East Rift Zone.

There is a steep gradient in both annual precipitation and groundwater recharge (fig. 7) across Kīlauea summit (the trade wind-rain shadow boundary). The oxygen ($\delta^{18}O$) and hydrogen (δD) stable isotope composition of rainfall varies substantially over a small (approximately 15 km^2) area (figs. 10 and 13; sites P24, P26, and P28). In the early 1990s, the stable-isotope composition in the NSF drill hole on the summit of Kīlauea was close to the average of the two nearest rain collectors, so that no flowpath is indicated for the NSF drill hole on figure 12 (where it is labelled G21). Samples collected later from the NSF drill hole (fig. 13) also indicate local recharge. Both stable-isotope data and spring temperatures (sites G19, G20) suggest that some heated groundwater from the Kīlauea summit area flows southward to shoreline springs (fig. 12).

Spatial and temporal trends in groundwater solute chemistry reflect mixing of fresh meteoric water, seawater, and magmatic volatiles, influenced by varying degrees of water-rock interaction. Perched, dike-impounded, and basal freshwater-lens groundwaters that are unaffected by seawater mixing or magmatic input are typically low-salinity sodium-bicarbonate waters (less than about 200 milligrams per liter [mg/L] of total dissolved solids [TDS]). The likelihood of seawater mixing increases with proximity to the shoreline and with depth. Because of the high salinity (34,500 mg/L TDS) of seawater, the major-ion chemistry of mixed waters that contain even a small fraction of seawater is mostly determined by the constituents in seawater (Janik and others, 1994).

Intense high-temperature geochemical signatures have been observed in samples taken during the course of geothermal development and operations at the Puna

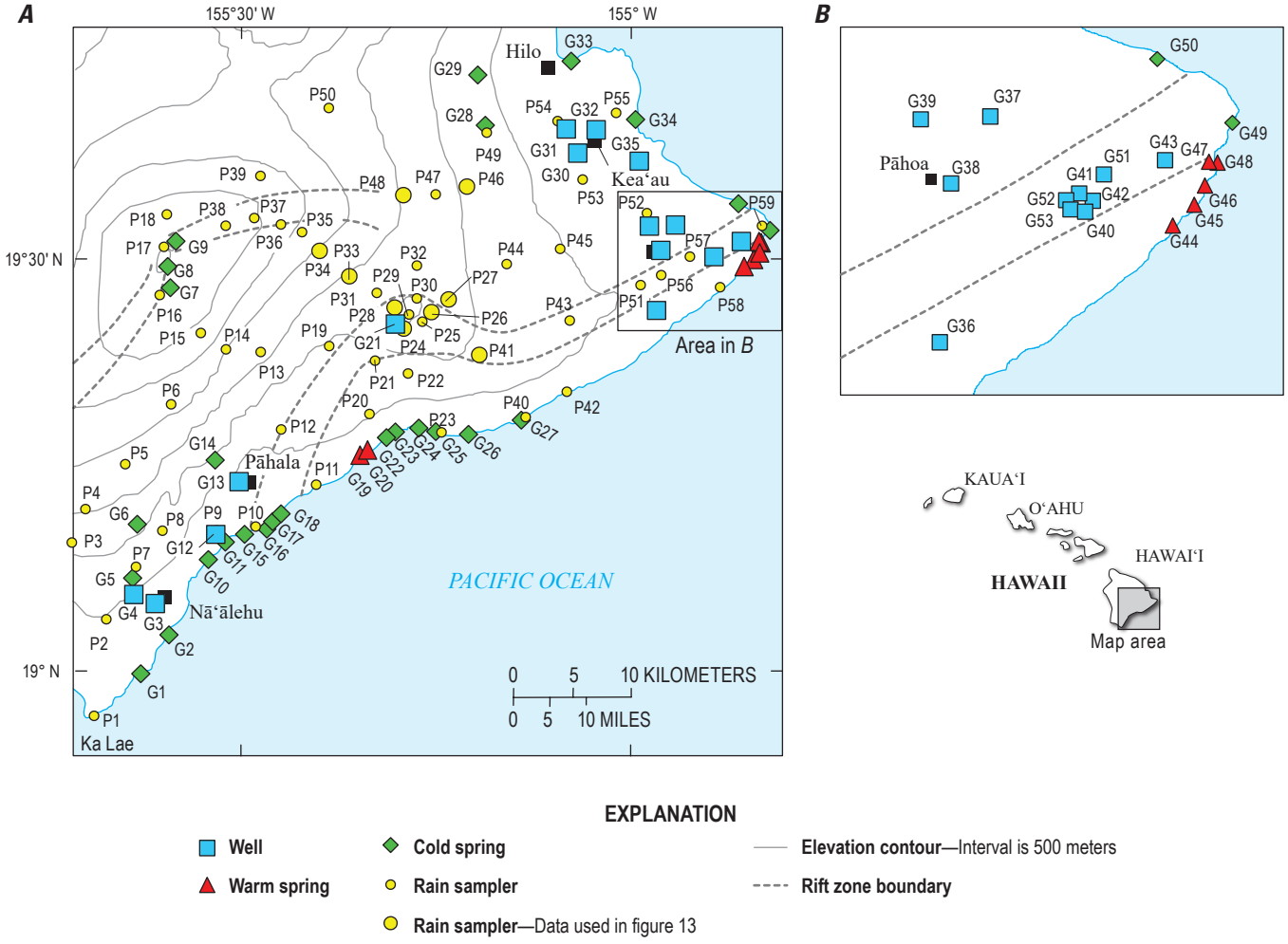

Figure 10. Map showing locations of precipitation (P1–P59) and groundwater (G1–G53) sample sites from Scholl and others' (1996) water-isotope study of the southeastern part of the Island of Hawai‘i.

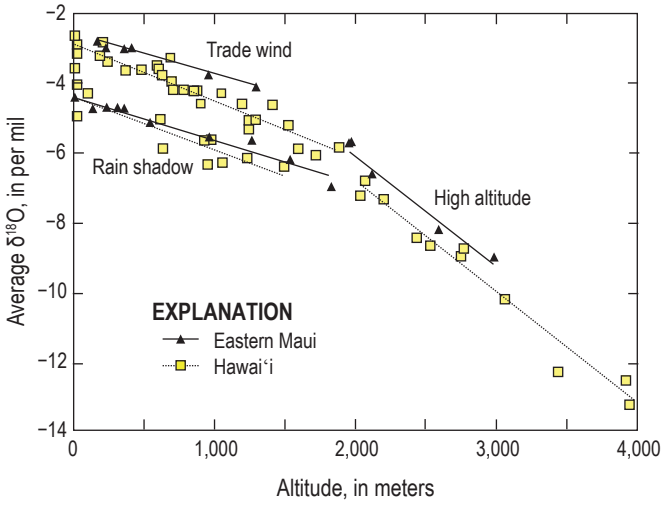

Figure 11. Plot showing volume-weighted average oxygen stable-isotope ($\delta^{18}O$) values versus elevation in the southeastern part of the Island of Hawai‘i (sample locations in fig. 10) and in eastern Maui in the vicinity of Haleakalā volcano. Stable isotope-elevation relations differ between trade-wind-dominated, rain-shadow, and high-elevation (more than 2,000 meters elevation) climatic zones. Figure after Scholl and others (2002).

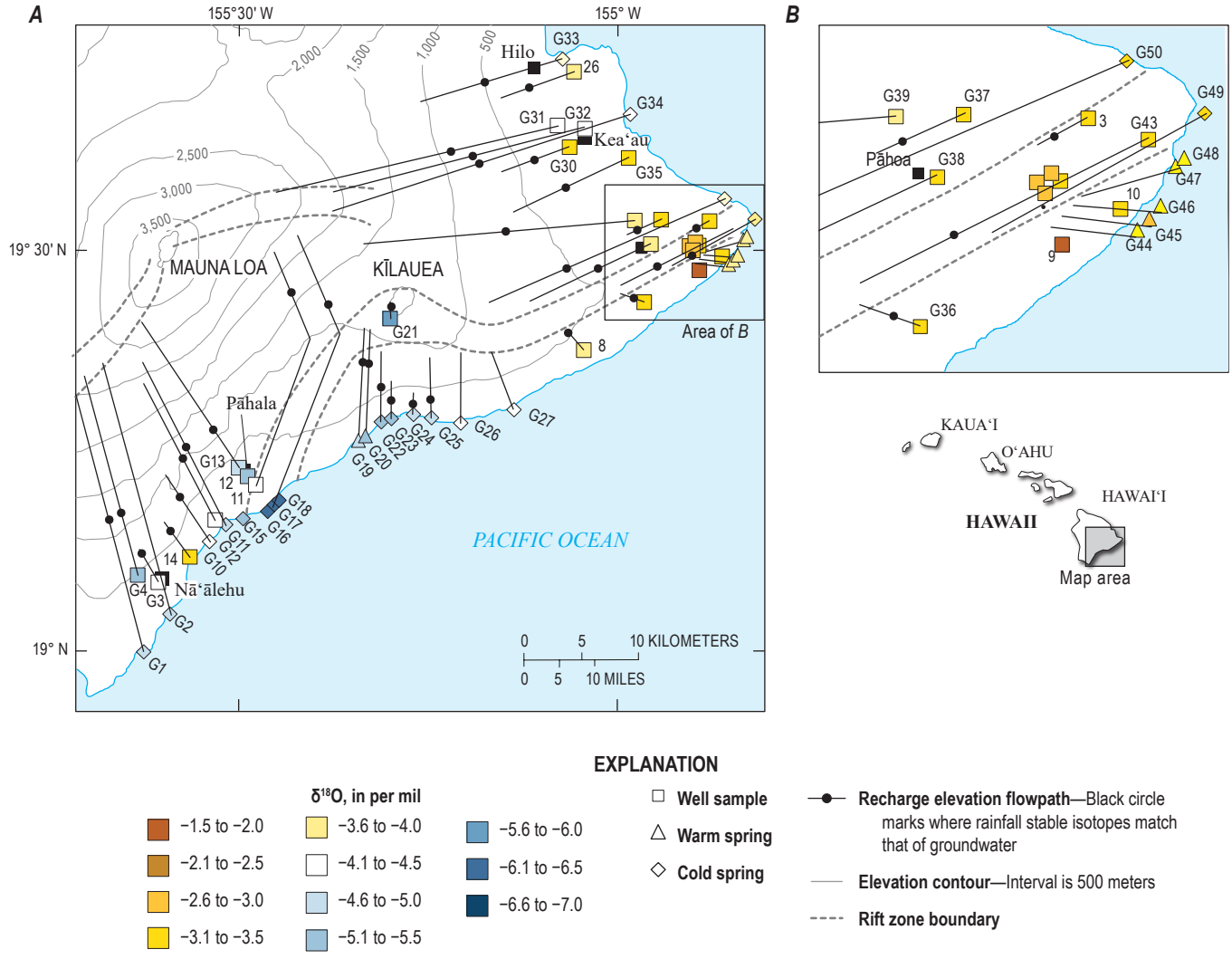

Figure 12. Map showing recharge elevations for groundwater samples calculated using the relation between rainfall oxygen stable-isotope composition ($\delta^{18}O$) and elevation (fig. 11). Lines extend from sample sites (colored symbols) to hypothetical maximum recharge elevations. Black circles on flow paths mark the elevation at which isotopic composition of rainfall matches that of groundwater measured at the site. Figure after Scholl and others (1996); stable-isotope data for sample sites 3, 8, 9, 10, 11, 12, 14, and 26 from McMurtry and others (1977).

Geothermal Venture in the lower East Rift Zone of Kīlauea (Kaleikini and others, 2011). Reconstruction of the deep reservoir fluid chemistry is somewhat complicated by the fact that geothermal production wells yield both steam and residual brine. The major-ion chemistry remains seawater-dominated (Janik and others, 1994; Evans and others, 2015). Several species, such as B, K, Li, Rb, and SiO_2, are notably enriched in the geothermal injectate and brine, whereas Mg is virtually absent. This pattern is a nearly universal characteristic of high-temperature geothermal systems worldwide (Giggenbach, 1988; Evans and others, 2015).

Almost no deep-reservoir geothermal signature is evident in nearby lower East Rift Zone springs or shallow thermal and nonthermal wells. The heat in springs (fig. 9*A*) and shallow thermal wells (fig. 9*B*) apparently moves by conduction from the geothermal reservoir into shallow groundwaters through a zone of low-permeability rock that largely blocks passage of geothermal water (Janik and others, 1994; Sorey and Colvard, 1994; Evans and others, 2015). One exception is a pair of monitoring wells (for example, MW-1; fig. 9) just above the producing reservoir at the Puna Geothermal Venture power plant (Kaleikini and others, 2011), where groundwater apparently absorbs H_2S gas from an underlying steam zone. The gas is then oxidized to sulfuric acid, which dissolves cations from reservoir minerals (Janik and others, 1994; Evans and others, 2015).

Some magmatic degassing occurs below Kīlauea's summit (Gerlach and Graeber, 1985) before volatile-depleted magma moves downrift. At the summit of Kīlauea, the interaction of magma and hot rock with groundwater, and the addition of gases released from the magma to water, may produce a variety of water compositions. Prior to emergence of the new crater lake in mid-2019, summit groundwater had been sampled only at the NSF drill hole (fig. 14), where it is relatively saline and rich in bicarbonate and sulfate. Whereas chloride in the lower East Rift Zone wells and springs is chiefly from seawater, this may not be the case at the summit, where the water table is approximately 600 m a.s.l. and the general covariance of sulfate (magmatic in origin) and chloride (figs. 14*A* and 14*B*) suggests a common, presumably magmatic source. The time-variance of summit groundwater chemistry may in part reflect varying degrees of volatile condensation and solution into groundwater (scrubbing; Symonds and others, 2001) as the underlying magma itself evolves (Lamy-Chappuis and others, 2020) and as focused, direct degassing is promoted by vent opening and the evolution of hot, vapor-dominated chimneys adjacent to magma columns.

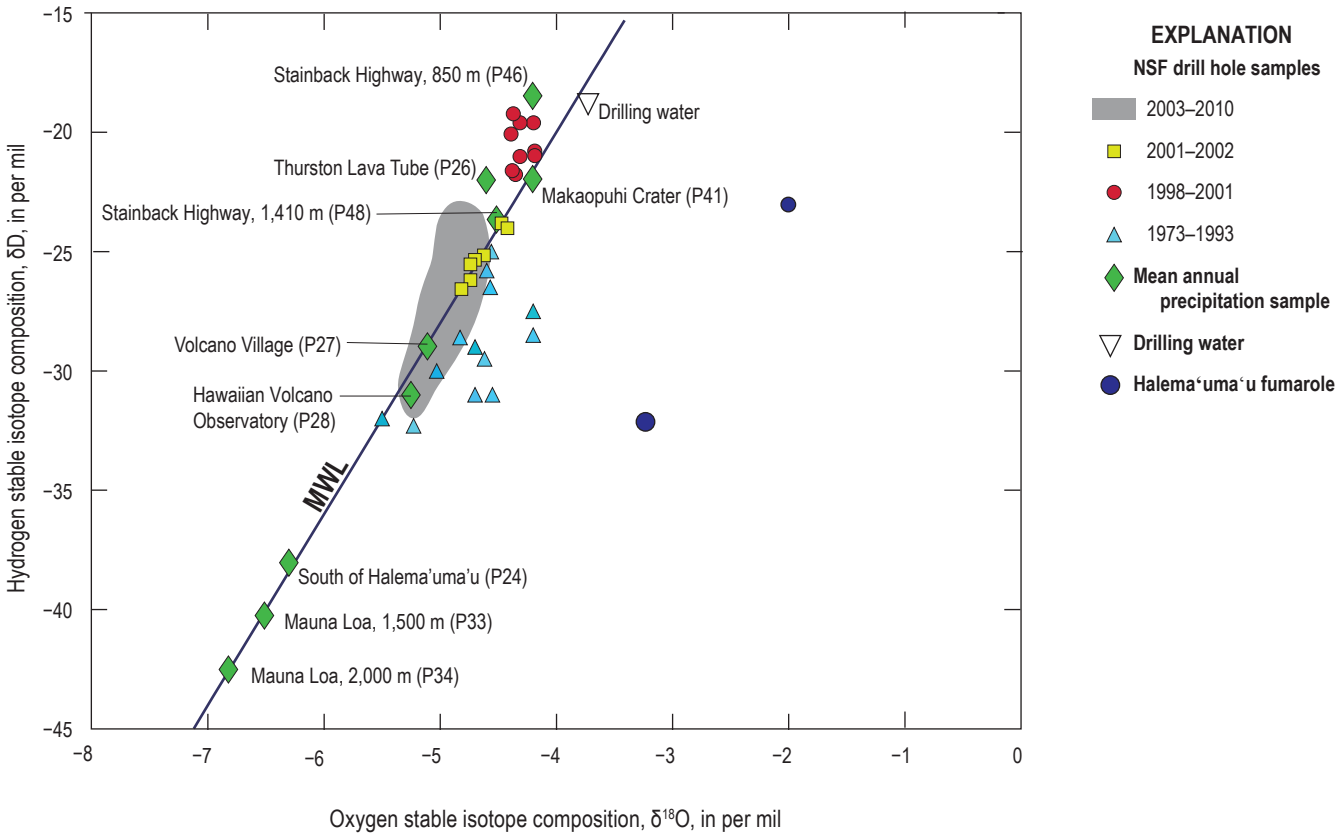

Figure 13. Plot of water-isotope composition of samples collected from the National Science Foundation (NSF) drill hole before and after the cleanout in 1998. Also shown are the compositions of drilling water from well PSM-1 south of Hilo (Tilling and Jones, 1996) and 300 °C fumaroles sampled at Halema‘uma‘u in the 1990s (Hinkley and others, 1995; Goff and McMurtry, 2000), the local meteoric water line (MWL; Scholl and others, 1996), and compositions of mean annual precipitation on and near Kīlauea (Scholl and others, 1996). See figure 10 for precipitation sampling locations. Figure after Hurwitz and others (2003).

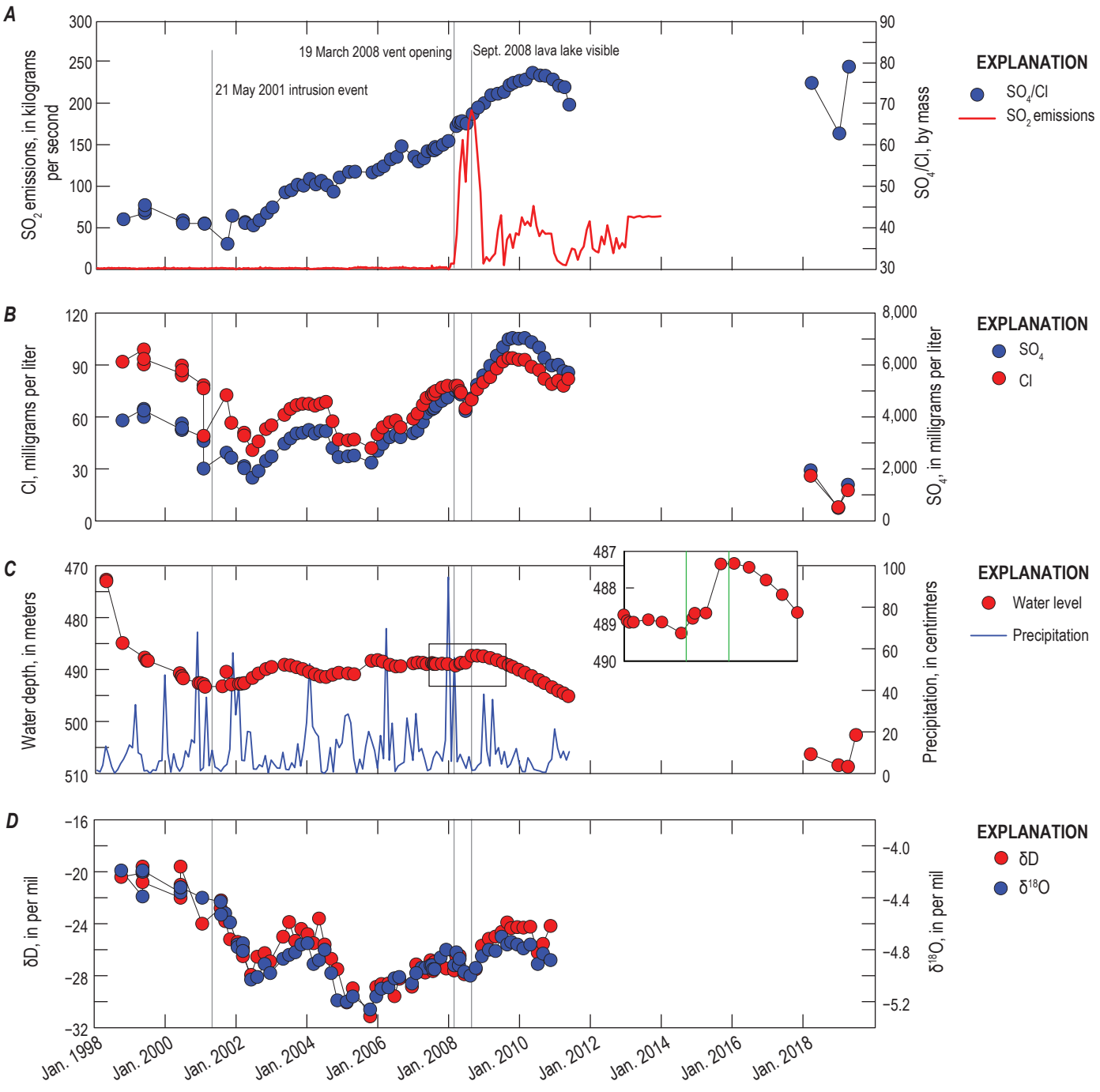

Figure 14. Plots of water-level and water-chemistry data from the National Science Foundation (NSF) drill hole and sulfur dioxide emissions from Kīlauea summit since the 1998 drill hole cleanout (fig. 15) until 2019. *A*, Kīlauea sulfur dioxide emissions and sulfate/chloride ratios in the NSF drill hole. *B*, Chloride and sulfate concentrations in the NSF drill hole. *C*, Water depth in the NSF drill hole and precipitation on Kīlauea. *D*, Hydrogen (δD) and oxygen ($\delta^{18}O$) stable isotope compositions. The intrusion event on May 21, 2001 (fig. 16), opening of the summit eruptive vent on March 19, 2008, and the initial glimpse of the lava lake in September 2008 are noted. The largest seismic event in 2008 was a nearby (1 kilometer [km] away), deep (approximately 25 km depth) magnitude 3.6 earthquake on February 6, 2008, and clearly predates the changes in water level, solute chemistry, and isotopic composition in mid-2008. External water was added to the drill hole on three occasions: September 10, 2000 (15–20 cubic meters [m^3]), January 17, 2001 (unknown amount), and July 6, 2004 (0.2 m^3), but had no obvious impact on the water-level and water-chemistry records. SO_2 emission data are from Elias and others (2020). Monthly precipitation from Hawaiian Volcano Observatory (station HAVO-OB, lat 19.4203° N., long 155.2881° W., elevation 1,215 meters).

Signatures and Impact of Volcano-Groundwater Interaction in Recent Decades

The deep NSF drill hole is particularly well located to monitor volcano-groundwater interaction. However, despite intermittent effort over several decades, large depth to water, high temperatures, aggressive water chemistry, and a narrow (5 centimeters [cm]) polyvinyl chloride access pipe have made it difficult to maintain a continuous, high-frequency record.

Elsewhere on Kīlauea Volcano, long-term hydrogeologic time series are sparse and mostly concentrated in the lower East Rift Zone, where selected records are maintained in the interests of public health (water-supply integrity) and to monitor the potential impact of geothermal development (Sorey and Colvard, 1994; Evans and others, 2015). Description and sampling of groundwater has been spatially comprehensive (Stearns and Clark, 1930; Stearns and Macdonald, 1946; Janik and others, 1994; Scholl and others, 1996), but highly intermittent. Systematic repeat measurements at a few sites have documented the presence or absence of transient changes over discrete time intervals through repeated geophysical surveys, temperature measurements, and water sampling.

Here our main focus is on observations made at the NSF drill hole on the summit of Kīlauea, and their implications for volcano-groundwater interactions, but we will also briefly summarize the sparse hydrogeologic time-series observations from elsewhere on the volcano.

Self-Potential Surveys

Self potential (SP) is a naturally occurring electric potential difference in the Earth, and fluids circulating through porous rock generate electric potentials that vary in space, time, and polarity (sign). Rapid decay of SP anomalies has been observed at Kīlauea summit after intrusions or eruptions (Zablocki, 1976; Jackson and others, 1985; Jackson, 1988), and large positive SP anomalies in the lower East Rift Zone (Zablocki, 1977) were important in locating the first successful geothermal production well. There are also many positive SP anomalies parallel to fissures within the upper Southwest Rift Zone (Jackson and Sako, 1979). Most large positive SP anomalies on Kīlauea are associated with subsurface localization of heat. Regional SP values show a negative correlation with topographic elevation and fluctuate with precipitation, and both effects are likely caused by groundwater recharge (Zablocki, 1978). Changes in hydrothermal systems can be sensed by both SP and resistivity techniques (Jackson, 1988), and systematic use of such techniques in a monitoring mode warrants further exploration (Lewicki and others, 2003).

Temperature Profiles

Temperature profiles in several Kīlauea drill holes, including the NSF drill hole on Kīlauea summit (figs. 5*A* and 15*B*), have been measured repeatedly over several decades. The temperature profiles from shallow wells in and south of the lower East Rift Zone reflect plumes of warmer, less-dense water floating on top of cooler, high-density water. The profiles were relatively stable between the 1970s and mid-1990s (Gingerich, 1995, p. 67), despite the nearby eruption in 1955. Thermal responses to various potential stimuli are commonly slow (figs. 6*A* and 6*B*), owing in part to the large thermal inertia of the rock mass.

Repeat Water Sampling in the Lower East Rift Zone

Systematic repeat water sampling has been done in the lower East Rift Zone to assess the possible impact of geothermal-energy development, including more than 20 years of monitoring conducted or overseen by the Hawai‘i State Department of Health and the Hawai‘i County Department of Water Supply (Janik and others, 1994; Sorey and Colvard, 1994; Evans and others, 2015). The apparent impact of geothermal development deep in the groundwater system on shallow groundwater, if any, is minimal. Two organic compounds (pentane and isopropanol) that are injected into the geothermal reservoir at the power plant have not been detected in groundwaters, other than a low concentration of pentane in one nearby deep monitoring well (Evans and others, 2015). This result is consistent with the view that the geothermal reservoir in the lower East Rift Zone is separated from shallow groundwaters by a zone of low-permeability rock.

Data from the NSF Drill Hole on Kīlauea Summit

The record from the NSF drill hole on Kīlauea summit is extensive; however, it mainly consists of low-frequency (for example, quarterly) water-level and geochemistry measurements, and there are major gaps. Further, prior to a cleanout operation in 1998, both the hydraulic response and the water chemistry of the NSF drill hole were likely affected by inflow of drilling mud from the surrounding formation, which limited access to hydrothermal fluids (Hurwitz and others, 2003). Bailing and drilling operations in the fall of 1998 cleared mud out of the drill hole to a depth of about 690 m, removing caked mud that may have been supporting a perched water layer in the well above the deep saturated zone penetrated by the well. This changed the isotopic signature (fig. 13) and solute chemistry (Tilling and Jones, 1996; Hurwitz and others, 2003) of waters sampled from the drill hole, and the water level subsequently declined by 12 m over 6 months, returning to the approximate level observed during the 1973 drilling (fig. 15*A*). Subsequent temperature profiles confirmed temperatures similar to those measured in 1973 (fig. 15*B*). Here we focus on post-1998 observations from the NSF drill hole.

Attempts to generate high-frequency water-level records in the NSF drill hole have largely been defeated by the large depth to water, high temperature, and aggressive water

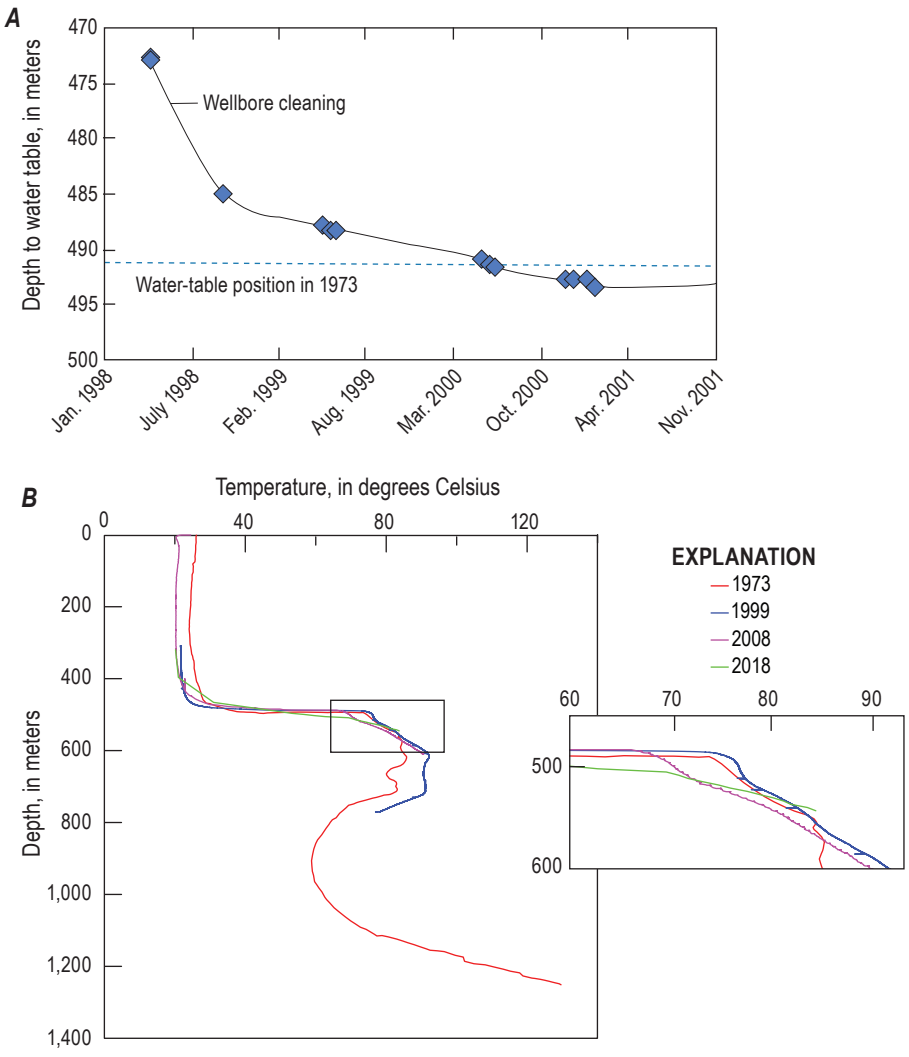

Figure 15. Plots of (*A*) water-level recovery after cleanout of the National Science Foundation (NSF) drill hole on Kīlauea summit in 1998 and (*B*) temperature profiles measured in the NSF drill hole from 1973 to 2018.

chemistry, but have yielded a few brief periods of record. During one such period in 2001, summit inflation caused by an intrusive event produced a rapid and large increase in compressional strain (fig. 16*A*) and a simultaneous water-level decline of 6 cm (fig. 16*B*). This mode of water-level change (drop) is opposite to that expected for compressional strain from poroelastic theory, and may reflect opening of fractures or interflows that drained water from the drill hole (Hurwitz and Johnston, 2003). Another brief period of high-frequency water-level record from 2009 shows that the NSF drill hole was still responsive to diurnal and semidiurnal loading of Earth tides and atmospheric pressure 11 years after the cleanout operation in 1998 (fig. 16*C*). The longer term water-level record maintained continuously from 2002 to 2011 (fig. 14*C*) consists of manual tape-down measurements at monthly to quarterly frequencies, and thus is not suited to capture small and brief strain responses like those seen in 2001. Many relatively small or brief water-level excursions like that observed in 2001 have likely occurred but are not reflected in the water-level record.

Increased SO_4^{2-} and Cl^- concentrations in the NSF drill hole starting in late 2005 (fig. 14*B*) may be a delayed response to the surge in magma supply during 2003–2007 (Poland and others, 2012), which resulted in degassing and subsequent scrubbing of magmatic SO_2 and HCl at shallow levels (hundreds of meters). The molar concentrations of SO_2 (2.89 percent) and HCl (0.047) in the Kīlauea gas plume (Oppenheimer and others, 2018) correspond to a SO_2/HCl mass ratio of 108 (SO_4/Cl = 166), which is higher than the ratio in the drill hole samples, suggesting either an increase of SO_2/HCl in the

gas plume as magma degases closer to the ground surface (Edmonds and others, 2013; Oppenheimer and others, 2018), preferential scrubbing of HCl, consistent with thermodynamic calculations (Symonds and others, 2001), or both.

The summit vent opening in 2008, which followed a 25-year hiatus in eruptive activity at Kīlauea summit (Orr and others, 2013), was the most significant change in local hydrogeologic conditions during the post-cleanout (1998–2018) period of record. Water levels, water chemistry, and stable-isotope composition changed in the NSF drill hole coincident with the period of vent opening and lava-lake appearance in mid-2008 (fig. 14; Hurwitz and others, 2019). The physical drivers of the observed suite of responses remain ambiguous. Similar excursions in water-level and groundwater-chemistry time series (for example, Skelton and others, 2014) have commonly been attributed to permeability changes caused by seismic activity (Ingebritsen and Manga, 2019). However, such responses are typically coseismic. The largest seismic event in 2008 was a nearby (1 km), deep (approximately 25 km depth) magnitude 3.6 earthquake on February 6, 2008, which clearly predates the changes in water level, solute chemistry, and isotopic composition in mid-2008. Other Kīlauea earthquakes in 2008 probably generated insufficient seismic energy density (less than 0.001 joules per cubic meter; Wang and Manga, 2010) and peak ground velocity (less than 0.2 centimeters per second; Elkhoury and others, 2006) to generate significant permeability changes.

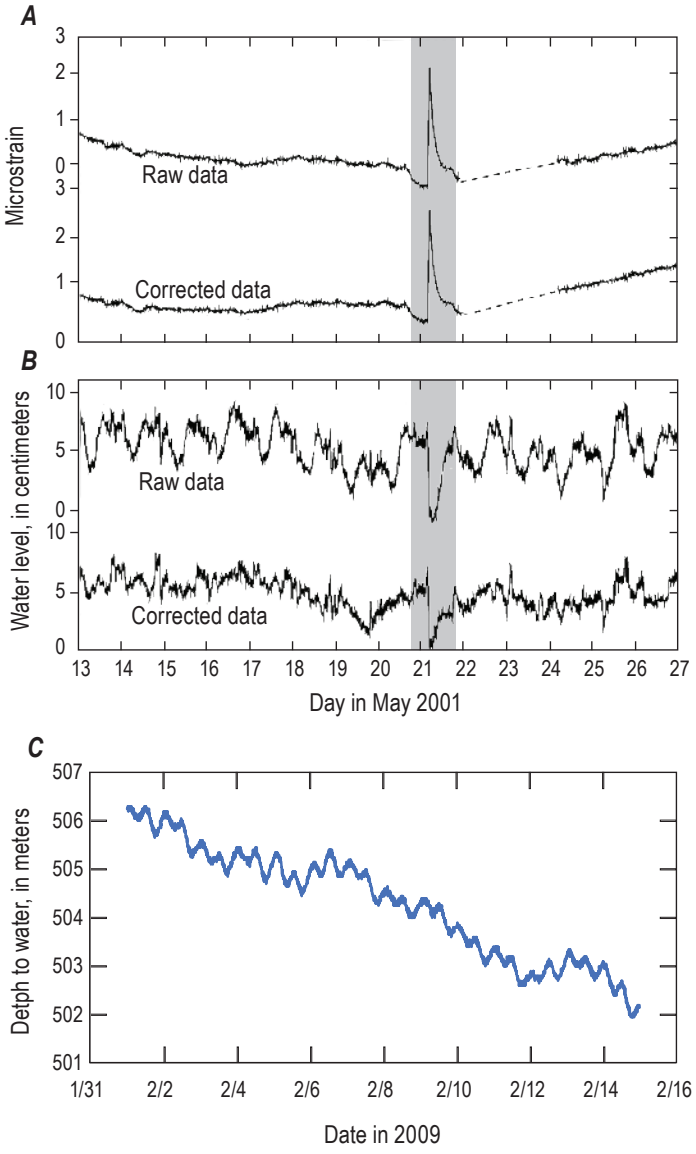

Figure 16. Plots of strain, water level, and depth to water in the National Science Foundation (NSF) drill hole on Kīlauea summit. *A*, Strain and, *B*, water-level measured spanning the May 21, 2001, intrusion event. Data are shown before (raw) and after correction for Earth tides and barometric pressure loading (from Hurwitz and Johnston, 2003). *C*, Raw water-level data from the NSF drill hole in early 2009.

The absence of a sufficiently strong seismic stimulus in mid-2008 suggests that contemporaneous observations in the NSF drill hole mainly reflect the changing nature of magma-groundwater interaction. However, interpretation of water levels and chemistry is further complicated by the low-frequency sampling rate, approximately monthly to bimonthly during that time (Hurwitz and others, 2019). The summit eruptive vent opened on March 19, 2008, and the lava lake became visible in September (Orr and others, 2013). Water level (fig. 14*C*) declined by approximately 1 m between February 27 and March 9, 2008, rose unsteadily by more than 2.5 m between March 9 and October 7, 2008, and then began a steady decline that was regularly measured through May 5, 2011. Measurements resumed in 2018 and suggest that the period of water-level decline may have persisted. The cumulative water-level decline in 2010–2018 was approximately 20 m. The initial change in major-ion concentrations (figs. 14*A* and 14*B*) was delayed relative to the water-level changes, declining by nearly 20 percent between March 21 and June 10, 2008, before resuming a systematic increase that was otherwise nearly continuous from early 2007 to mid-2010. Observed variations in stable-isotope compositions (fig. 14*D*) are more complex, but δD values ranged from −26.5 to −28.0 per mil (‰) through October 7, 2008, and ranged from −23.9 to −26.2 ‰ thereafter—a shift toward less-depleted (heavier) isotopic composition.

Decreasing solute concentrations beginning about October 7, 2010 (fig. 14*B*), with less apparent change in the SO_4/Cl ratio (fig. 14*A*), may reflect lagged response to the vent opening in 2008. We speculate that condensation and dissolution of volatiles in the groundwater system was fairly widespread during the 25-year hiatus in eruptive activity at the summit and that, from 2008 on, volcanic-volatile discharge became focused into the vicinity of the now-open vent (fig. 17*A*). With continuing low-salinity recharge input, groundwater then became progressively more dilute. The

large increase in summit SO_2 emissions in 2008 (fig. 14*A*) is consistent with shallow degassing, and an increase in bulk outgassing (Elias and Sutton, 2012), but may also reflect transition from a scrubbing-dominated regime to vapor-phase volatile discharge. The gradual growth of a vapor-dominated zone impermeable to liquid flow (discussed further below) may have further isolated the magma conduit, and vapor-phase upflow, from liquid groundwater. Under this scenario, the approximately 2-year time lag between the emergence of the lava lake in 2008 and the systematic decrease in solute concentrations from 2010 to present provides some indication of the solute-transport timescale between the lava lake and the approximately 1.5-km-distant NSF drill hole.

Numerical Modeling of Groundwater Flow and Heat Transport

The 2018 Kīlauea eruption (fig. 17*A*) prompted numerical-modeling studies of multiphase flow, heat transport, and transient behavior in the summit groundwater system. Previous data and modeling studies from the NSF drill hole (figs. 5, 6, 13, and 14) provided essential constraints.

The renewed interest in the summit groundwater system in early 2018 owed largely to an influential conceptual model based on the explosive 1924 eruption (fig. 17*B*). This model postulates that the 1924 explosions were triggered by liquid-water inflow into a recently vacated magma conduit. In early

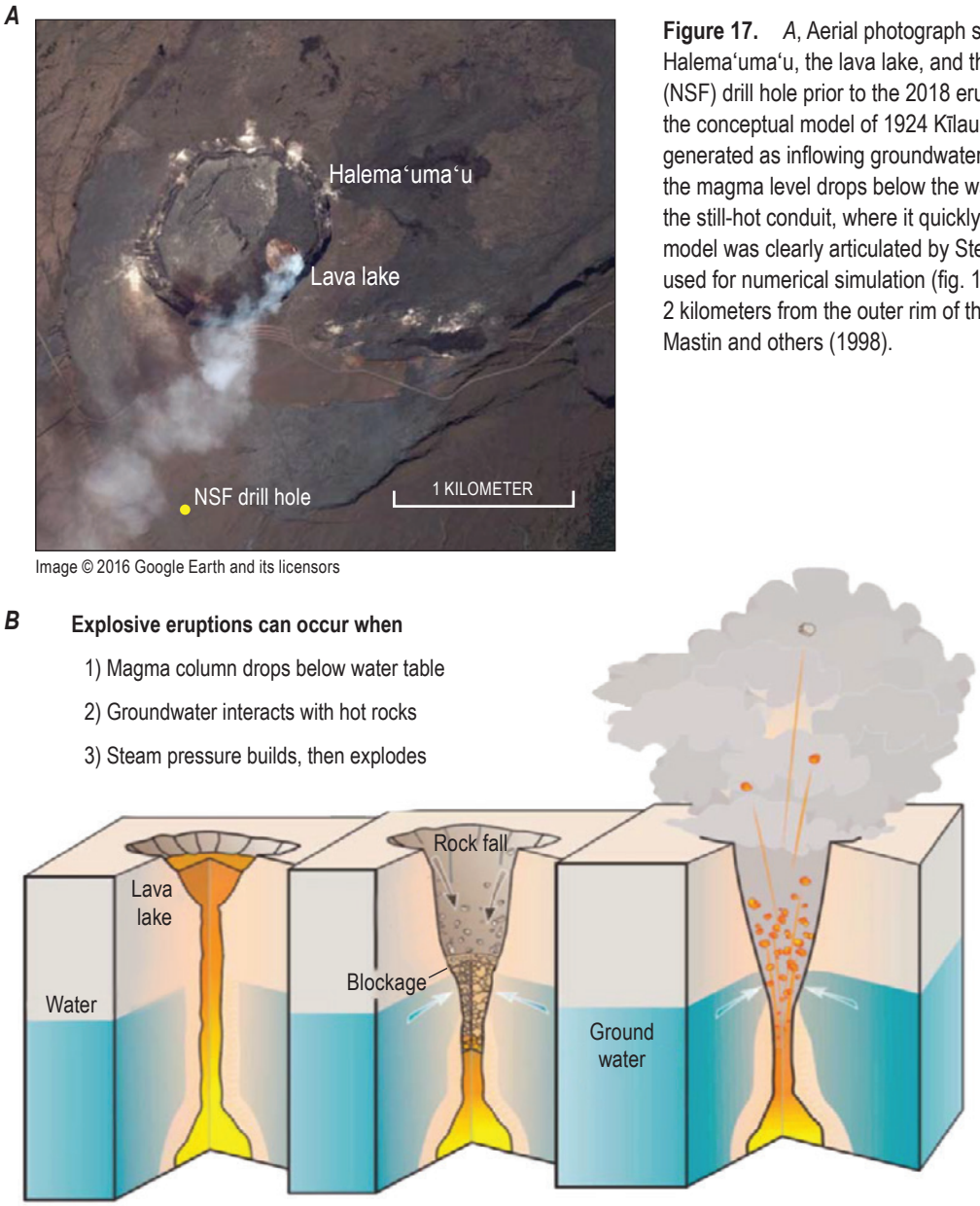

Figure 17. *A*, Aerial photograph showing relative positions of Halemaʻumaʻu, the lava lake, and the National Science Foundation (NSF) drill hole prior to the 2018 eruption sequence. *B*, Diagram showing the conceptual model of 1924 Kīlauea explosions powered by steam generated as inflowing groundwater came in contact with hot rocks. Once the magma level drops below the water table, groundwater can flow into the still-hot conduit, where it quickly flashes to steam. This conceptual model was clearly articulated by Stearns (1925). The geometric model used for numerical simulation (fig. 18) extends radially outward for 2 kilometers from the outer rim of the lava lake. Figure modified from Mastin and others (1998).

May 2018, magma in Kīlauea's summit reservoir system was rapidly being evacuated toward the volcano's East Rift Zone (Neal and others, 2019). This caused a rapid (approximately 2 m per hour) decrease in the height of the summit lava lake, which was projected to drop below the approximate water-table position on about May 11. The onset of explosive activity was considered a strong possibility both in light of the 1924 eruption model and the fact that, for 1,500 of the past 2,500 years, Kīlauea's eruptions were dominantly explosive, manifested by repeated phreatic and phreatomagmatic activity in a deep summit caldera (Swanson and others, 2014). Modeling exercises were performed to explore the groundwater-flow regime near the magma conduit (Hsieh and Ingebritsen, 2019).

The numerical-modeling exercises done on May 10–14, 2018, yielded a more nuanced view of the classic conceptual model and possible causes of the subsequent explosions. The results demonstrated that liquid-water inflow to the magma conduit could potentially be delayed by months to years. The modeling exercises employed the U.S. Geological Survey HYDROTHERM model (visit https://volcanoes.usgs.gov/software/hydrotherm for more information), an open-source code that simulates multiphase fluid and heat transport over the relevant temperature range (0–1,200 °C) (Kipp and others, 2008).

Permeability is the single most important parameter governing potential inflow of groundwater. The conceptual model proposed for the 1924 summit eruption assumed permeability similar to that of shallow, unaltered Hawaiian basalts (Stearns, 1925), which are among the most permeable geological materials on Earth, with horizontal permeability on the order of 10^{-10} m^2, comparable to that of karst limestone, well-sorted sand, or gravel. The layering of lava flows introduces some anisotropy, and limited well-test data in Hawaiian lavas suggest vertical permeability (k_z) perhaps 10–200 times less than horizontal permeability (k_x). The actual permeabilities beneath the water table on Kīlauea summit are now known to be quite different. Murray (1974, p. 56–61) estimated the permeability of the interval from 500–1,200 m depth in the NSF drill hole to be 1×10^{-14} m^2 on the basis of mud loss rates during drilling, and inferred a value of 6×10^{-14} m^2 from numerical-modeling experiments that simulated convection within a rectangular model and matched the distinctive temperature profile (fig. 6*A*). The mud-loss-based permeability value for the NSF drill hole (1×10^{-14} m^2) is an estimate of horizontal permeability, whereas the model-based value (6×10^{-14} m^2) assumes isotropic conditions. Both values are significantly larger than the permeability of core samples obtained in that interval (approximately 5×10^{-17} m^2; fig. 5*A*), but discrepancies of such magnitude (10^3 to 10^4) between core measurements and in situ or inferred values are commonly observed in fractured crystalline rocks (Brace, 1980, p. 247). The conceptual model proposed for the 1924 eruption also assumed a near-sea-level water table beneath Kīlauea summit (Stearns, 1925), whereas the water table is now known to be at approximately 600 m elevation.

The simulations considered k_x values of 10^{-13} to 10^{-14} m^2 and a range of anisotropies. It was particularly important to explore high-side permeability values in order to assess the possibility of rapid liquid-water inflow. However, if permeability is inversely correlated to temperature, as seems to be the case in most hydrothermal systems (Bjornsson and Bodvarsson, 1990), the actual permeabilities near Halema‘uma‘u may be even lower than those documented at the NSF drill hole—that is, k_x less than 10^{-14} m^2. Permeabilities on the order of $k_x = k_z \leq 10^{-16}$ m^2 are needed to maintain elevated pore-fluid pressures in geologic media (for example, see Neuzil, 1995), so fluid pressures in the simulations were generally near hydrostatic.

Important and irreducible modeling uncertainties are associated with the longevity and geometry of magma conduits beneath Halema‘uma‘u and (or) the lava lake (fig. 17*A*). The modeling exercises experimented with heating durations ranging from 10 years (the age of the lava lake) to 100 years (the approximate time since the explosive 1924 eruption) and with magma-conduit radii ranging from 50 m (less than the small axis of the lava lake) to 400 m (the approximate pre-eruption radius of Halema‘uma‘u). A nominal model thickness (depth) of 200 m was adopted, corresponding to the hot "aquifer" zone mapped below the water table at the NSF drill hole (figs. 5*A*, 6, and 15*B*). This thickness is consistent with the continuous lateral flow model (fig. 6*B*) but is otherwise rather arbitrary; it has little qualitative influence on the results.

Modeling was done in cylindrical coordinates (fig. 18). In the general case, we expect some lateral flow owing to regional groundwater head gradients. At Kīlauea summit, groundwater flow is generally southward toward the coast from the higher, wetter north side of the caldera (fig. 12). Regional groundwater gradients could cause asymmetric heating and cooling that cannot be represented in cylindrical coordinates. However, the regional gradients are likely smaller than those induced locally by the effects of the magma conduit.

The upper boundary of the model at 0.1 megapascals (1 bar) and 90 °C represents conditions at the water table as observed at the NSF drill hole. The lower boundary is closed to heat and fluid flow. The distal boundary is placed at sufficiently large distance so as not to influence the results (as much as 2 km radial distance), and maintained at 90 °C and hydrostatic pressures. An inner cylinder that represents the magma conduit is maintained at 1,000 °C for 10–100 years, then drained instantaneously, after which the face of the magma conduit is maintained at atmospheric pressure and 90 °C, permitting water inflow.

The heating stage prior to the 2018 magma drainage is of primary interest here. A steam zone (no mobile liquid water) develops around the magma conduit within 1 year (fig. 19). The steam zone is approximately 30 m wide after 10 years

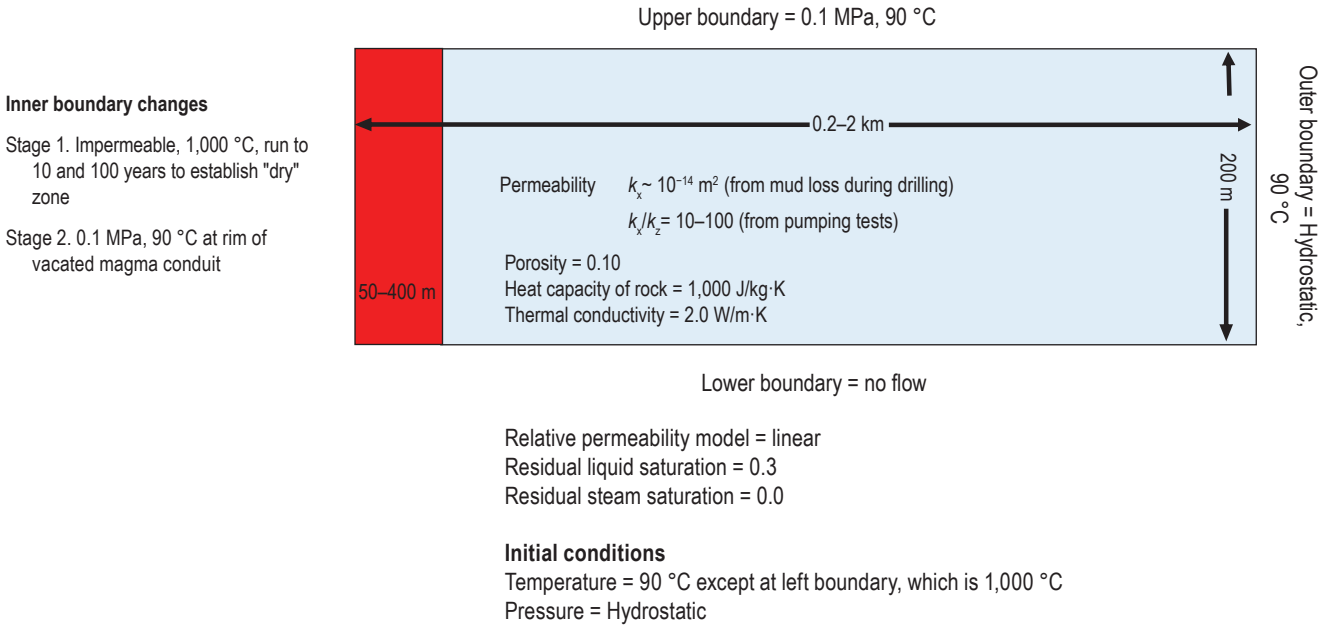

Figure 18. Geometry, boundary and initial conditions, and key parameters for numerical modeling of radial groundwater inflow toward a preheated volcanic conduit. The change in the inner (left) boundary from stage 1 to stage 2 represents the presence of magma followed by instantaneous drainage of a conduit filled with magma at 1,000 °C. During stage 1, the inner boundary is closed to fluid flow but open to heat flow, and fluid pressures near the magma conduit are generally near hydrostatic, controlled by the upper- and outer-boundary pressures. During stage 2, the inner boundary is open to fluid flow, and fluid pressures near the vacated magma conduit are generally subhydrostatic. Relative permeabilities are invoked in multiphase flow simulations to represent the reduction in mobility of one fluid phase owing to the interfering presence of other phases. They are treated as scalar functions of liquid volume saturation (V_{liquid}/V_{void}), and the linear function and residual saturation values invoked here are standard defaults for steam and liquid water flow (for example, Ingebritsen and others, 2006). Abbreviations: m, meter; m^2, square meter; km, kilometer; °C, degree Celsius; MPa, megapascals; J/kg·K, joules per kilogram per kelvin; W/m·K, watts per meter per kelvin.

(fig. 20*A*) for both the wide and narrow conduits; its width is essentially independent of conduit radius. After 100 years (fig. 20*B*), the steam zone is approximately 100 m wide in both cases. The length and time dimensions of the predrainage steam zone are controlled largely by heat conduction from the magma conduit—lateral advection of heat has little obvious effect. The existence of the steam zone is incorporated in the conceptual model of figure 17*B* and by Stearns (1925), who invoked a "gas cushion surrounding the magma." However, its inhibiting effect on liquid groundwater inflow had not been fully appreciated. The simulation results revealed that, contrary to expectations, liquid water inflow to the drained conduit would likely be delayed by months to years (3–24 months), owing to the inability of liquid water to transit the zone of very hot rock surrounding the conduit.

We have speculated that decreasing solute concentrations beginning on about October 7, 2010 (fig. 14*B*), reflect a lagged response to the vent opening in 2008, which allowed comparatively free release of magmatic volatiles that had previously condensed and dissolved into the groundwater system. The growing vapor-dominated zone adjacent to the magma conduit may also have acted to restrict interaction between magmatic volatiles and liquid groundwater. Within 1 year after magma emplacement, there is predicted to be no mobile liquid water within approximately 10 m of the magma conduit (see flow vectors in fig. 19), and, by 10 years after emplacement, there is no mobile liquid water within approximately 30 m of the magma (fig. 20). Volatiles could flow up through the growing vapor-dominated chimney without encountering liquid water and escape to the atmosphere without much scrubbing.

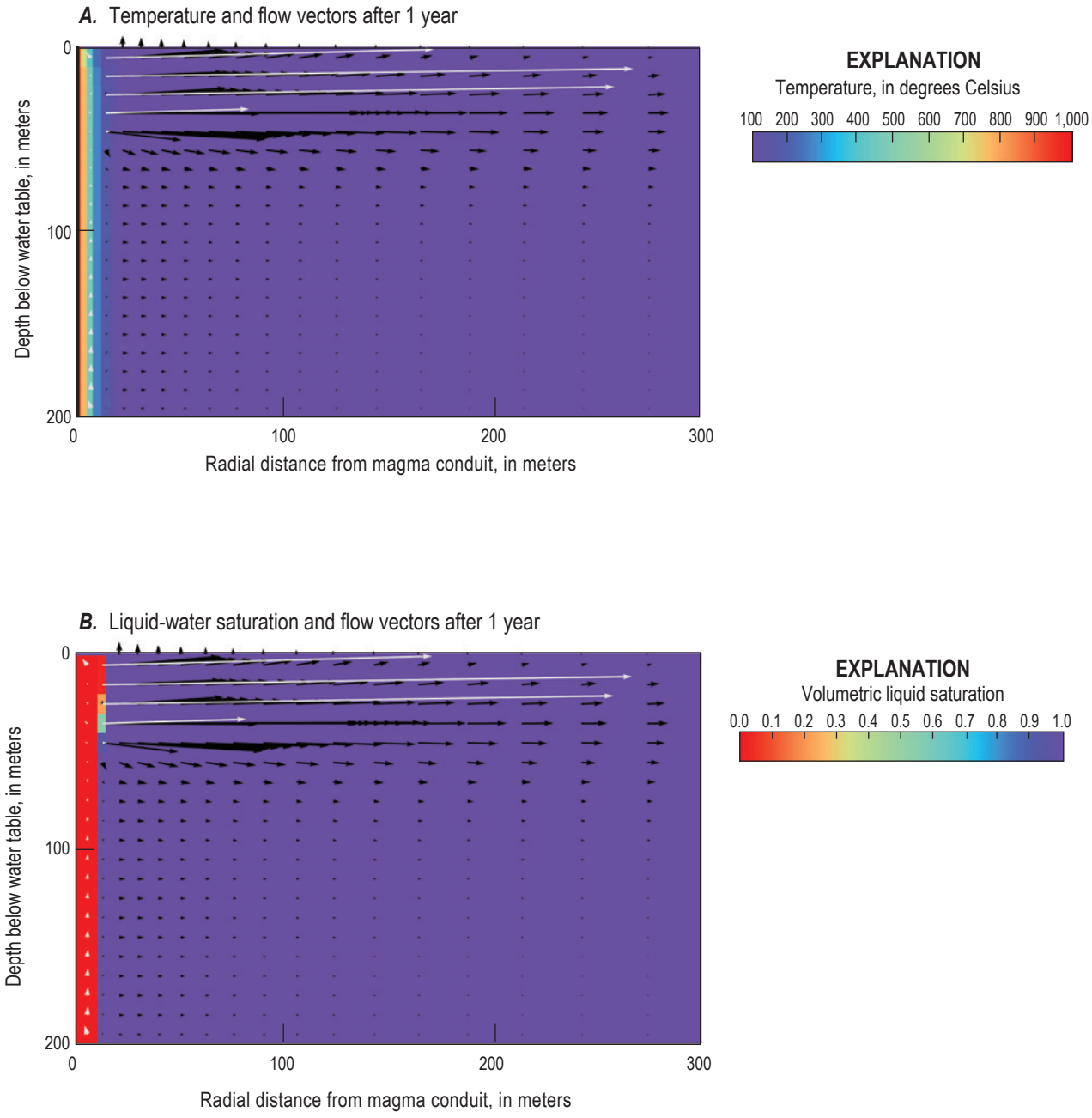

Figure 19. Plots of radial numerical model results after 1 year of heating by a narrow (50-meter radius) magma conduit. *A*, Temperature and flow vectors. *B*, Liquid-water saturation and flow vectors. As the magma conduit heats the surrounding basalt, water evolves to a two-phase mixture (0 < saturation < 1) and eventually to pure steam (saturation = 0). Water expansion causes outward flow (away from the magma conduit) and a small amount of upward flow to the water table (upper boundary). Black lines are liquid-water flow vectors, and small black squares denote their origins. White lines are steam-flow vectors and are illustrated as ten times longer than the water flow vectors (for the same mass flow rate). Vectors are plotted on every other column of cells to enhance visibility.

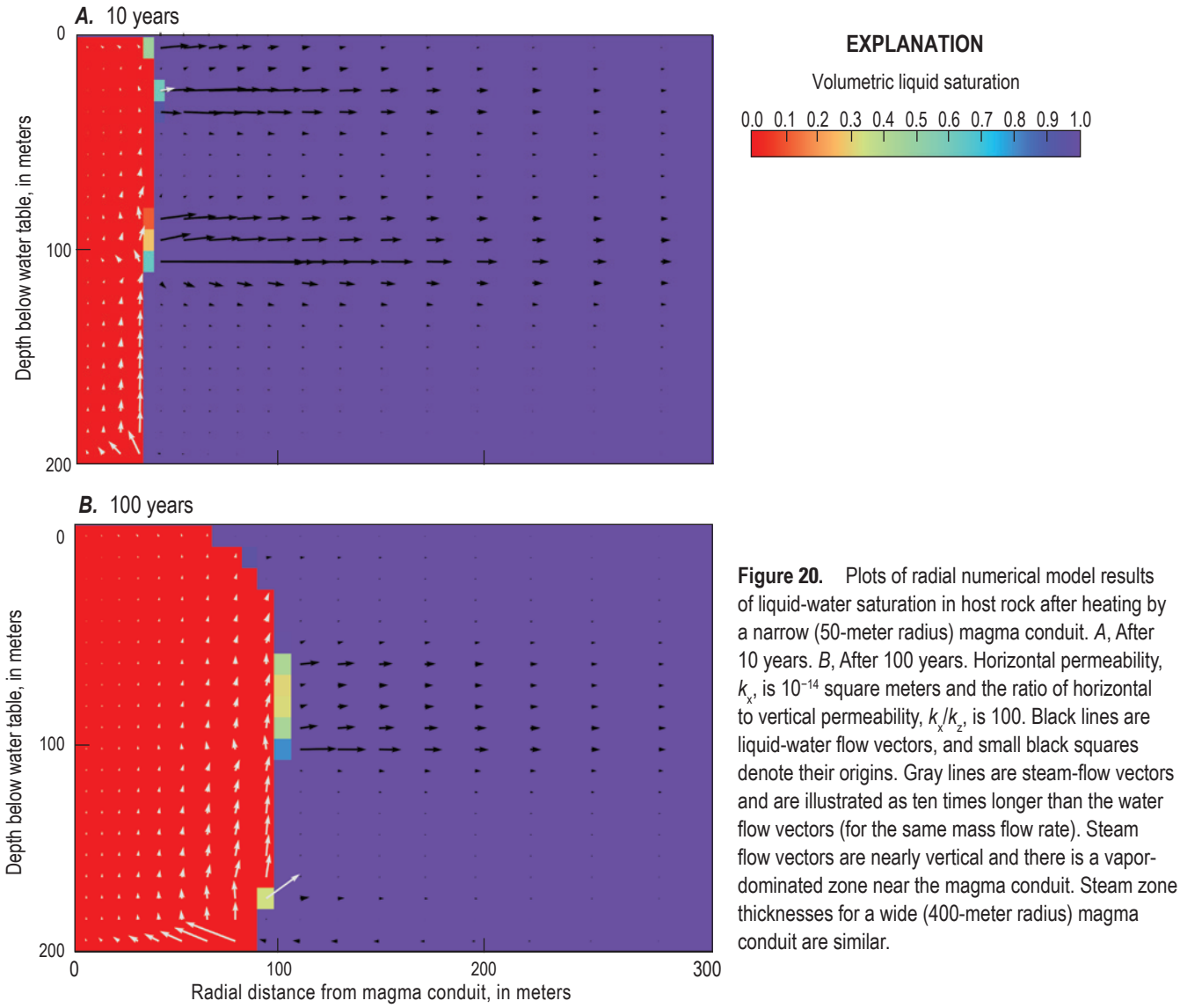

Figure 20. Plots of radial numerical model results of liquid-water saturation in host rock after heating by a narrow (50-meter radius) magma conduit. *A*, After 10 years. *B*, After 100 years. Horizontal permeability, k_x, is 10^{-14} square meters and the ratio of horizontal to vertical permeability, k_x/k_z, is 100. Black lines are liquid-water flow vectors, and small black squares denote their origins. Gray lines are steam-flow vectors and are illustrated as ten times longer than the water flow vectors (for the same mass flow rate). Steam flow vectors are nearly vertical and there is a vapor-dominated zone near the magma conduit. Steam zone thicknesses for a wide (400-meter radius) magma conduit are similar.

Discussion and Open Questions

Despite the 2011–2018 data gap, solute concentrations in the NSF drill hole on Kīlauea summit can be seen to have declined systematically from 2010 to present (figs. 14*A* and 14*B*). If we assume that the decline in sulfate (SO_4^{2-}) concentrations observed in the NSF drill hole (from approximately 7,000 to 1,000 mg/L; fig. 14*B*) is representative of groundwater caldera-wide (approximately 10 km^2), we can calculate the total mass change in dissolved sulfur in the subsurface. We further assume, as in the numerical models, a porosity of 10 percent and that active flow and transport (in this case, the decline in SO_4^{2-}) was mainly restricted to the uppermost 200 m of the groundwater system below the water table, because of lower permeabilities at greater depths (figs. 5 and 6). Under these assumptions, the caldera-wide decline would amount to approximately 4×10^5 metric tons of sulfur. This quantity is equivalent to approximately 3–4 years of the early-2008 summit-plume sulfur emissions, prior to vent opening, 60 days of the highest rate (April–November 2008) emissions, or 240 days of 2009–2013 emissions (based on SO_2-emission data from Elias and others [2020]). Because this simple first-order calculation relies on a single sampling point, the uncertainty is both large and difficult to quantify. However, the results suggest a large capacity of this highly active groundwater system to absorb and transport volcanic volatiles, consistent with observations that more than 90 percent of solute discharge (Schopka and Derry, 2012), approximately 95 percent of groundwater discharge (Stearns and Macdonald, 1946), and approximately 99 percent of the discharge of intrusion-supplied heat occurs offshore.

There are unanswered questions about the connectivity between the NSF drill hole on Kīlauea summit and the surrounding groundwater system, and to what extent

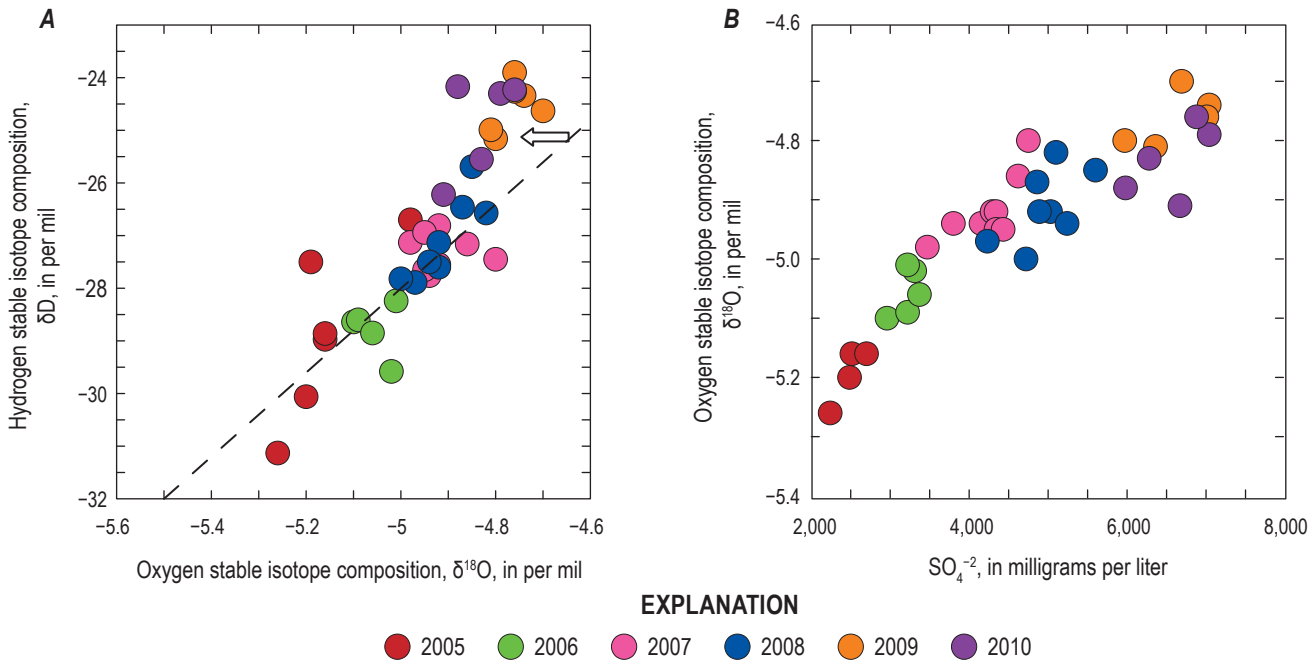

Figure 21. Plots of water stable-isotopic composition in the National Science Foundation (NSF) drill hole on Kīlauea summit. *A*, Hydrogen (δD) and oxygen ($\delta^{18}O$) stable-isotopic composition of water samples grouped by year. Dashed line shows the local meteoric water line of Scholl and others (1996). Arrow indicates the predicted direction of change resulting from oxygen-isotope exchange between SO_4^{2-} and H_2O (Chiba and Sakai, 1985); arrow length is the analytical precision of $\delta^{18}O$ analyses. *B*, Relation between $\delta^{18}O$ and SO_4^{2-} concentrations, showing the significant increase in SO_4^{2-} concentrations and coincident increase in $\delta^{18}O$ values between 2005 and 2007, during the accelerated inflation of Kīlauea summit prior to vent opening in mid-2008. From Hurwitz and Anderson (2019).

conditions in the NSF drill hole can serve as a caldera-wide proxy. In early 1998, both the hydraulic response and the water chemistry changed substantially after bailing and drilling operations cleared mud from the drill hole (Hurwitz and others, 2003). There is some indication that major-ion concentrations (Hurwitz and others, 2019) have generally trended back toward pre-1998 conditions since 2007. The abundance of bicarbonate relative to sulfate and chloride generally increased from 2009 to 2018, potentially consistent with interaction between isolated, CO_2-charged groundwater and residual drilling mud. Assessment of this possibility is complicated by the absence of cation data after October 7, 2008. Whether the water level still responds to periodic loading, as it did, for example, in 2001 and 2009 (fig. 16), is unknown. We note however that the pre-1998 mud clogging was associated with an artificially elevated water level (fig. 15*A*), whereas the water level declined substantially from 2010 to 2018 (fig. 14*C*).

Finally, there was a systematic change in the stable-isotope composition of water samples from the NSF drill hole sometime in the mid-1990s, from generally below the local meteoric water line of Scholl and others (1996) in 1973–1993 to generally above that line in 1998–2010 (figs. 13 and 21; Hurwitz and others, 2019). This shift is generally consistent with changes seen in lower East Rift Zone samples between the early 1990s and early 2010s, which were tentatively attributed to a shift in the local meteoric water line (Evans and others, 2015). There is also strong covariance between $\delta^{18}O$ and SO_4^{2-} concentrations in 2005–2010 samples from the NSF drill hole (fig. 21). This covariance cannot be fully explained by oxygen exchange between sulfate ions and water (Chiba and Sakai, 1985) because, even at the highest observed concentrations, the oxygen atoms in SO_4^{2-} would only be ~0.5 percent as abundant as the oxygen atoms in H_2O. That δD shows the same or similar covariance, and that the isotopic compositions trend along the local meteoric water line, further seems to rule out major oxygen-isotopic exchange with SO_4^{2-}. The observed covariance may instead reflect mixing of shallower and deeper groundwaters (Hurwitz and Anderson, 2019). The fact that post-2001 isotopic data points are generally collinear with the local meteoric water line on $\delta^{18}O$-δD plots, such as figures 13 and 21, suggests ongoing communication with the surrounding groundwater system.

References Cited

Beirle, S., Hörmann, C., Penning de Vries, M., Dörner, S., Kern, C., and Wagner, T., 2014, Estimating the volcanic emission rate and atmospheric lifetime of SO_2 from space—A case study for Kīlauea volcano, Hawai‘i: Atmospheric Chemistry and Physics, v. 14, p. 8,309–8,322, https://doi.org/10.5194/acp-14-8309-2014.

Blackwell, D.D., 1994, A summary of deep thermal data from the Cascade Range and analysis of the "rain curtain" effect: Oregon Department of Geology and Mineral Industries Open-File Report O-94-07, p. 75–131.

Blackwell, D.D., and Baker, S.L., 1988, Thermal analysis of the Austin and Breitenbush geothermal systems, Western Cascades, Oregon, *in* Sherrod, D.R., ed., Geology and geothermal resources of the Breitenbush and Austin Hot Springs area, Clackamas and Marion Counties, Oregon: Oregon Department of Geology and Mineral Industries Open-File Report O-88-5, p. 47–62.

Bjornsson, G., and Bodvarsson, G., 1990, A survey of geothermal reservoir properties: Geothermics, v. 19, p. 17–27.

Bouhifd, M.A., Besson, P., Courtial, P., Gerardin, C., Navrotsky, A., and Richet, P., 2007, Thermochemistry and melting properties of basalt: Contributions to Mineralogy and Petrology, v. 153, p. 689–698, https://doi.org/10.1007/s00410-006-0170-8.

Brace, W.F., 1980, Permeability of crystalline and argillaceous rocks: International Journal of Rock Mechanics and Mining Science and Geomechanics Abstracts, v. 17, p. 241–251.

Bredehoeft, J.D., and Papadopulos, I.S., 1965, Rates of vertical groundwater movement estimated from the Earth's thermal profile: Water Resources Research, v. 1, p. 325–328.

Burns, E.R., Williams, C.F., Ingebritsen, S.E., Voss, C.I., Spane, F.A., and DeAngelo, J., 2015, Understanding heat and groundwater flow through continental flood basalt provinces—Insights gained from alternative models of permeability/depth relationships for the Columbia Plateau, USA: Geofluids, v. 15, p. 120–138, https://doi.org/10.1111/gfl.12095.

Buttner, G., and Huenges, E., 2003, The heat transfer in the region of the Mauna Kea (Hawaii)—Constraints from borehole temperature measurements and coupled thermo-hydraulic modeling: Tectonophysics, v. 371, p. 23–40.

Chiba, H., and Sakai, H., 1985, Oxygen isotope exchange rate between dissolved sulfate and water at hydrothermal temperatures: Geochimica et Cosmochimica Acta, v. 49, p. 993–1,000, https://doi.org/10.1016/0016-7037(85)90314-X.

Clague, D.A., Hagstrum, J.T., Champion, D.E., and Beeson, M.H., 1999, Kilauea summit overflows—Their ages and distribution in the Puna District, Hawaii: Bulletin of Volcanology, v. 61, p. 363–381.

Edmonds, M., Sides, I.R., Swanson, D.A., Werner, C., Martin, R.S., Mather, T.A., Herd, R.A., Jones, R.L., Mead, M.I., Sawyer, G., and Roberts, T.J., 2013, Magma storage, transport and degassing during the 2008-10 summit eruption at Kīlauea Volcano, Hawai'i: Geochimica et Cosmochimica Acta, v. 123, p. 284–301.

Elias, T., Kern, C., Sutton, A.J., and Horton, K., 2020, Sulfur dioxide emission rates from Kīlauea Volcano, Hawaii, 2008–2013: U.S. Geological Survey data release, https://doi.org/10.5066/P9K0EZII.

Elias, T., and Sutton, A.J., 2012, Sulfur dioxide emission rates from Kīlauea Volcano, Hawai'i, 2007–2010: U.S. Geological Survey Open-File Report 2012–1107, 25 p.

Elkhoury, J.E., Brodsky, E.E., and Agnew, D.C., 2006, Seismic waves increase permeability: Nature, v. 441, p. 1,135–1,138.

Engott, J.A., 2011, A water-budget model and assessment of groundwater recharge for the Island of Hawai'i: U.S. Geological Survey Scientific Investigations Report 2011–5078, 53 p.

Evans, W.C., Bergfeld, D., Sutton, A.J., Lee, R.C., and Lorenson, T.D., 2015, Groundwater chemistry in the vicinity of the Puna Geothermal Venture power plant, Hawai'i, after two decades of production: U.S. Geological Survey Scientific Investigations Report 2015–5139, 26 p.

Fischer, W.A., Davis, D.A., and Sousa, T.M., 1966, Freshwater springs of Hawaii from infrared images: U.S. Geological Survey Hydrologic Investigations Atlas HA-218.

Flinders, A.F., Ito, G., Garcia, M.O., Sinton, J.M., Kauahikaua, J.P., and Taylor, B., 2013, Intrusive dike complexes, cumulate cores, and the extrusive growth of Hawaiian volcanoes: Geophysical Research Letters, v. 40, p. 3,367–3,373, https://doi.org/10.1002/grl.50633.

Gerlach, T.M., and Graeber, E.J., 1985, Volatile budget of Kilauea volcano: Nature, v. 313, p. 273–277.

Giggenbach, W.F., 1988, Geothermal solute equilibria derivation of Na-K-Mg-Ca geoindicators: Geochimica et Cosmochimica Acta, v. 52, p. 2,749–2,765.

Gingerich, S.B., 1995, The hydrothermal system of the lower East Rift Zone of Kilauea Volcano—Conceptual and numerical models of energy and solute transport: University of Hawai'i, Ph.D. dissertation, OMI no. 9615520.

Goff, F., and McMurtry, G.M., 2000, Tritium and stable isotopes of magmatic waters: Journal of Volcanology and Geothermal Research, v. 97, p. 347–396.

Harris, R.N., Von Herzen, R.P., McNutt, M.K., Garven, G., and Jordahl, K., 2000, Submarine hydrogeology of the Hawaiian archipelagic apron—1. Heat flow patterns north of Oahu and Maro Reef: Journal of Geophysical Research, v. 105, p. 21,353–21,369.

Hildebrand, T.G., Rosenbaum, J.G., and Kauahikaua, J.P., 1993, Aeromagnetic study of the Island of Hawaii: Journal of Geophysical Research, v. 98, p. 4,099–4,119.

Hinkley, T.K., Quick, J.E., Gregory, R.T., and Gerlach, T.M., 1995, Hydrogen and oxygen isotopic compositions of waters from fumaroles at Kilauea summit, Hawaii: Bulletin of Volcanology, v. 57, p. 44–51.

Horai, K.I., 1991, Thermal conductivity of Hawaiian basalt—A new interpretation of Robertson and Peck's data: Journal of Geophysical Research, v. 96, p. 4,125–4,132.

Hsieh, P.A., and Ingebritsen, S.E., 2019, Groundwater inflow toward a preheated volcanic conduit—Application to the 2018 eruption at Kīlauea volcano, Hawai‘i: Journal of Geophysical Research, v. 124, p. 1,448–1,506, https://doi.org/10.1029/2018JB017133.

Hulen, J.B., and Lutz, S.J., 1999, Altered volcanic rocks as hydrologic seals on the geothermal system of Medicine Lake volcano, California: Geothermal Resources Council Bulletin, v. 7, p. 217–222.

Hurwitz, S., and Anderson, K.R., 2019, Temporal variations in scrubbing of magmatic gases at the summit of Kīlauea Volcano, Hawai‘i: Geophysical Research Letters, v. 46, no. 24, p. 14,469–14,476, https://doi.org/10.1029/2019GL085904.

Hurwitz, S., Goff, F., Janik, C.J., Evans, W.C., Counce, D.A., Sorey, M.L., and Ingebritsen, S.E., 2003, Mixing of magmatic volatiles with groundwater and interaction with basalt on the summit of Kilauea Volcano, Hawaii: Journal of Geophysical Research, v. 108, 12 p., https://doi.org/10.1029/2001JB001594.

Hurwitz, S., Ingebritsen, S.E., and Sorey, M.L., 2002, Episodic thermal perturbations associated with groundwater flow—An example from Kilauea Volcano, Hawaii: Journal of Geophysical Research, v. 107, 10 p., https://doi.org/10.1029/2001JB001654.

Hurwitz, S., and Johnston, M.J.S., 2003, Groundwater level changes in a deep well in response to a magma intrusion event on Kilauea Volcano, Hawai‘i: Geophysical Research Letters, v. 30, 4 p., https://doi.org/10.1029/2003GL018676.

Hurwitz, S., Peek, S., Younger, E.F., and Lee, R.L., 2019, Water level, temperature, and chemistry in a deep well on the summit of Kīlauea Volcano, Hawai‘i: U.S. Geological Survey data release, https://doi.org/10.5066/P9UCGT2F.

Hussong, D.M., and Cox, D.C., 1967, Estimation of groundwater configuration near Pahala, Hawaii, using electrical resistivity techniques: Honolulu, University of Hawai‘i Water Resources Research Center Technical Report 17, 35 p.

Ingebritsen, S.E., and Manga, M., 2019, Earthquake hydrogeology: Water Resources Research, v. 55, 5 p., https://doi.org/10.1029/2019WR025341.

Ingebritsen, S.E., Sanford, W.E., and Neuzil, C.E., 2006, Groundwater in Geologic Processes: Cambridge University Press, 536 p.

Ingebritsen, S.E., and Scholl, M.A., 1993, The hydrogeology of Kilauea Volcano: Geothermics, v. 22, p. 255–270.

Izuka, S.K., Engott, J.A., Rotzoll, K., Bassiouni, M., Johnson, A.G., Miller, L.D., and Mair, A., 2018, Volcanic aquifers of Hawai‘i—Hydrogeology, water budgets, and conceptual models: U.S. Geological Survey Scientific Investigations Report 2015–5164, 158 p.

Jackson, D.B., 1988, Geoelectrical observations (including the September 1982 summit eruption), chap. 8 *of* Wolfe, E.W., ed., The Puu Oo erution of Kilauea Volcano, Hawaii—Episodes 1 through 20, January 3, 1983, through June 8, 1984: U.S. Geological Survey Professional Paper 1463, p. 237–251.

Jackson, D.B., Kauahikaua, J.P., and Zablocki, C.J., 1985, Resistivity monitoring of an active volcano using the controlled-source electromagnetic technique: Journal of Geophysical Research, v. 90, p. 12,545–12,555.

Jackson, D.B., and Sako, M., 1979, Self-potential mapping on the southwest rift zone of Kilauea volcano [abs.]: Hilo, Hawai‘i, Hawaiian Symposium on Intraplate Volcanism and Submarine Volcanism [July 22] abstract, p. 165.

Janik, C.J., Nathenson, M., and Scholl, M.A., 1994, Chemistry of well and spring waters on Kilauea Volcano, Hawaii: U.S. Geological Survey Open-File Report 94-586, 166 p.

Kaleikini, M., Spielman, P., and Buchanan, T., 2011, Puna geothermal venture 8MW expansion: Geothermal Resources Council Transactions, v. 35, p. 1,313–1,314.

Kauahikaua, J.P., 1993, Geophysical characteristics of the hydrothermal systems of Kilauea Volcano, Hawai‘i: Geothermics, v. 22, p. 271–299.

Keller, G.V., Grose. L.T., Murray, J.C., and Skokan, C.K., 1979, Results of an experimental drill hole at the summit of Kilauea Volcano, Hawaii: Journal of Volcanology and Geothermal Research, v. 5, p. 345–385.

Kipp, K.L., Hsieh, P.A., and Charlton, S.R., 2008, Guide to the revised ground-water flow and heat transport simulator; HYDROTHERM—Version 3: U.S. Geological Survey Techniques and Methods 6–A25, 160 p.

Lamy-Chappuis, B., Heinrich, C.A., Driesner, T., and Weis, P., 2020, Mechanisms and patterns of magmatic fluid transport in cooling hydrous intrusions: Earth and Planetary Science Letters, v. 535, 11 p.

Lewicki, J.L., Connor, C., St-Amand, K., Stix, J., and Spinner, W., 2003, Self—potential, soil CO_2 flux, and temperature on Masaya volcano, Nicaragua: Geophysical Research Letters, v. 15, 4 p., https://doi.org/10.1029/2003GL017731.

Martin, W.F., and Pierce, C.H., 1913, Water resources of Hawaii 1909–1911: U.S. Geological Survey Water-Supply Paper 318, 552 p.

Mastin, L.G., Christiansen, R.L., Swanson, D.A., Stauffer, P.H., and Hendley, J.W., 1998, Explosive eruptions at Kilauea Volcano, Hawaii?: U.S. Geological Survey Fact Sheet 132-98, 2 p.

McMurtry, G.M., Fan, P.F., and Coplen, T.B., 1977, Chemical and isotopic investigations of groundwater in potential geothermal areas in Hawaii: American Journal of Science, v. 277, p. 438–458.

Murray, J.C., 1974, The geothermal system at Kilauea Volcano, Hawaii: Golden, Colorado School of Mines, Ph.D. dissertation, OSTI identifier no. 7257596.

Neal, C.A., Brantley, S.R., Antolik, L., Babb, J.L., Burgess, M., Calles, K., Cappos, M., Change, J.C., Conway, S., Desmither, L., Dotray, P., Elias, T., Fukunaga, P., Fuke, S., Johanson, I.A., Kamibayashi, K., Kauahikaua, J., Lee, R.L., Pekalib, S, Miklius, A., Million, W., Moniz, C.J., Nadeau, P.A., Okubo, P., Parcheta, C., Patrick, M.R., Shiro, B., Swanson, D.A., Tollett, W., Trusdell, F., Younger, E.F., Zoeller, M.H., Montgomery-Brown, E.K., Anderson, K.R., Poland, M.P., Ball, J.L., Bard, J., Coombs, M., Dietterich, H.R., Kern, C., Thelen, W.A., Cervelli, P.F., Orr, T., Houghton, B.F., Gansecki, C., Hazlett, R., Lundgren, P., Diefenbach, A.K., Lerner, A.H., Waite, G., Kelly, P., Clor, L., Werner, C., Mulliken, K., Fisher, G., and Damby, D., 2019, The 2018 rift eruption and summit collapse of Kīlauea Volcano: Science, v. 363, p. 367–374.

Neuzil, C.E., 1995, Abnormal pressures as hydrodynamic phenomena: American Journal of Science, v. 295, p. 742–786.

Oppenheimer, C., Scaillet, B., Woods, A., Sutton, A.J., Elias, T., and Moussallam, Y., 2018, Influence of eruptive style on volcanic gas emission chemistry and temperature: Nature Geoscience, v. 11, p. 678–681.

Orr, T.R., Thelen, W.A., Patrick, M.R., Swanson, D.A., and Wilson, D.C., 2013, Explosive eruptions triggered by rockfalls at Kīlauea volcano, Hawai‘i: Geology, v. 41, p. 207–210, https://doi.org/10.1130/G33564.1.

Peterson, F.L., 1981, Geological and hydrological framework—A history of development, *in* Fujimura, F.N., and Chang, W.B.C., eds., Groundwater in Hawaii—A Century of Progress: Manoa, University Press of Hawaii, p. 1–14.

Pierce, H.A., and Thomas, D.M., 2009, Magnetotelluric and audiomagnetotelluric groundwater survey along the Humu’ula portion of Saddle Road near and around the Pohakuloa Training Area, Hawaii: U.S. Geological Survey Open-File Report 2009–1135, 160 p.

Poland, M.P., Miklius, A., Sutton, A.J., and Thornber, C.R., 2012, A mantle-driven surge in magma supply to Kīlauea Volcano during 2003-2007: Nature Geoscience, v. 5, p. 295–300.

Revil, A., Ghorbani, A., Gailler, L.S., Gresse, M., Cluzel, N., Panwar, N. and Sharma, R., 2018, Electrical conductivity and induced polarization investigations at Kilauea volcano, Hawai‘i: Journal of Volcanology and Geothermal Research, v. 368, p. 31–50.

Rotzoll, K., and El-Kadi, A.I., 2008, Estimating hydraulic conductivity from specific capacity for Hawaii aquifers, USA: Hydrogeology Journal, v. 16, p. 969–979.

Rotzoll, K., El-Kadi, A.I., and Gingerich, S.B., 2007, Estimating hydraulic properties for volcanic aquifers using constant-rate and variable-rate aquifer tests: Journal of the American Water Resources Association, v. 43, p. 334–345.

Saar, M.O., and Manga, M., 2004, Depth dependence of permeability in the Oregon Cascades inferred from hydrogeologic, thermal, seismic, and magmatic modeling constraints: Journal of Geophysical Research, v. 109, B04204, 19 p., https://doi.org/10.1029/2003JB002855.

Scholl, M.A., Gingerich, S.B., and Tribble, G.W., 2002, The influence of microclimates and fog on stable isotope signatures used in interpretation of regional hydrology—East Maui, Hawaii: Journal of Hydrology, v. 264, p. 170–184.

Scholl, M.A., Ingebritsen, S.E., Janik, C.J., and Kauahikaua, J.P., 1995, An isotope hydrology study of the Kilauea volcano area, Hawaii: U.S. Geological Survey Water-Resources Investigations Report 95-4213, 44 p.

Scholl, M.A., Ingebritsen, S.E., Janik, C.J., and Kauahikaua, J.P., 1996, Use of precipitation and groundwater isotopes to interpret regional hydrology on a tropical volcanic island—Kilauea volcano area, Hawaii: Water Resources Research, v. 32, p. 3,525–3,537.

Schopka, H.H., and Derry, L.A., 2012, Chemical weathering fluxes from volcanic islands and the importance of groundwater—The Hawaiian example: Earth and Planetary Science Letters, v. 339, p. 67–78.

Sclater, J.G., Jaupart, C., and Galson, D., 1980, The heat flow through oceanic and continental crust and the heat loss of the Earth: Reviews of Geophysics and Space Physics, v. 18, p. 269–311.

Skelton, A., Andrén, M., Kristmannsdottir, H., Stockmann, G., Mörth, C.-M., Sveinbjörnsdóttir, A., Jónsson, S., Sturkell, E., Gudrunardottir, H.R., Hjartarson, H., Siegmund, H., and Kockum, I., 2014, Changes in groundwater chemistry before two consecutive earthquakes in Iceland: Nature Geoscience, v. 7, p. 752–756.

Sorey, M.L., and Colvard, E.M., 1994, Potential effects of the Hawai‘i Geothermal Project on ground-water resources on the Island of Hawai‘i: U.S. Geological Survey Water-Resources Investigations Report 94-4028, 35 p.

Stearns, H.T., 1925, The explosive phase of Kilauea Volcano, Hawaii, in 1924: Bulletin Volcanologique, v. 2, no. 2, p. 194–208, https://doi.org/10.1007/BF02719505.

Stearns, H.T., and Clark, W.O., 1930, Geology and water resources of the Kau District, Hawaii: U.S. Geological Survey Water-Supply Paper 616, 194 p.

Stearns, H.T., and Macdonald, G.A., 1946, Geology and ground-water resources of the Island of Hawaii: Hawaii Division of Hydrography Bulletin 9, 362 p.

Stolper, E.M., DePaolo, D.J., and Thomas, D.M., 2009, Deep drilling into a mantle plume volcano—The Hawaii Scientific Drilling Project: Scientific Drilling, no. 7, p. 4–14, https://doi.org/10.2204/iodp.sd.7.02.2009.

Swanberg, C.A., Walkey, W.C., and Combs, J., 1988, Core hole drilling and the “rain curtain” phenomenon at Newberry Volcano, Oregon: Journal of Geophysical Research, v. 93, p. 10,163–10,173.

Swanson, D.A., 1972, Magma supply rate at Kilauea Volcano, 1952-1971: Science, v. 175, p. 169–170, https://doi.org/10.1126/science.175.4018.169.

Swanson, D.A., Rose, T.R., Mucek, A.E., Garcia, M.O., Fiske, R.S., and Mastin, L.G., 2014, Cycles of explosive and effusive eruptions at Kīlauea Volcano, Hawai‘i: Geology, v. 42, p. 631–634.

Symonds, R.B., Gerlach, T.M., and Reed, M.H., 2001, Magmatic gas scrubbing—Implications for volcano monitoring: Journal of Volcanology and Geothermal Research, v. 108, p. 303–341.

Takasaki, K.J., 1993, Ground-water occurrence in Kilauea Volcano and adjacent parts of Mauna Loa Volcano: U.S. Geological Survey Open-File Report 93-82, 28 p.

Thomas, D.M., Haskins, E., Pierce, H.A., and the Humu’ula Groundwater Project Team, 2015, New insights into the influence of structural controls affecting groundwater flow and storage within an ocean island volcano, Mauna Kea, Hawaii [abs.]: Eos Transactions American Geophysical Union, Fall Meeting Supplement, abstract H31D-1446.

Thomas, D.M., Wallin, E., and Lautze, N., 2014, A blind hydrothermal system in an ocean island environment—Humu’ula Saddle Hawaii Island [abs.]: Eos Transactions American Geophysical Union, Fall Meeting Supplement, abstract V21A-4731.

Tilling, R.I., and Jones, B.F., 1996, Waters associated with an active basaltic volcano, Kilauea, Hawaii—Variation in solute sources, 1973-1991: Geological Society of America Bulletin, v. 108, p. 562–577.

Torgerson, C.E., Faux, R.N., McIntosh, B.A., Poage, N.J., and Norton, D.J., 2001, Airborne thermal remote sensing for water temperature assessment in rivers and streams: Remote sensing of Environment, v. 76, p. 386–398.

von Herzen, R.P., Cordery, M.J., Detrick, R.S., and Fang, C., 1989, Heat flow and the thermal origin of hot spot swells—The Hawaiian swell revised: Journal of Geophysical Research, v. 94, p. 13,783–13,799.

Wang, C-Y., and Manga, M., 2010, Hydrologic responses to earthquakes and a general metric: Geofluids, v. 10, p. 206–216, https://doi.org/10.1111/j.1468-8123.2009.00270.x.

Williams, J.A., and Soroos, R.L., 1973, Evaluation of methods of pumping test analysis for application to Hawaiian aquifers: Honolulu, University of Hawai‘i Water Resources Research Center Technical Report 20, 159 p.

Wright, T.L., Peck, D.L., and Shaw, H.R., 1976, Kilauea lava lakes—Natural laboratories for study of cooling, crystallization, and differentiation of basaltic magma: American Geophysical Union Geophysical Monograph Series, v. 19, p. 375–390.

Zablocki, C.J., 1976, Mapping thermal anomalies on an active volcano by self-potential methods, Kilauea, Hawai‘i: U.N. Symposium on the Development and Use of Geothermal Resources, v. 2, p. 1,299–1,309.

Zablocki, C.J., 1977, Self-potential studies in East Puna, Hawai‘i: Hawai‘i Institute of Geophysics Technical Report HIG-77-15, p. 175–195.

Zablocki, C.J., 1978, Applications of the VLF induction method for studying some volcanic processes of Kilauea volcano, Hawai‘i: Journal of Volcanology and Geothermal Research, v. 3, p. 155–195.

Zablocki, C.J., Tilling, R.I., Peterson, D.W., Christiansen, R.L., Keller, G.V., and Murray, J.C., 1974, A deep research drill hole at the summit of an active volcano, Kilauea volcano, Hawaii: Geophysical Research Letters, v. 1, p. 323–326.

Moffett Field Publishing Service Center, California
Manuscript approved September 30, 2020
Edited by Monica Erdman
Cover design by Cory Hurd and layout by Kimber Petersen

ISSN 1044-9612 (print)
ISSN 2330-7102 (online)
https://doi.org/10.3133/pp1867F